

Kombolgie VTEM™ AEM Survey: Inversion Report

Geoscience Australia
GeoCat 72582

by

R.C. Brodie and M.T. Costelloe



Australian Government

Geoscience Australia

APPLYING GEOSCIENCE TO AUSTRALIA'S
MOST IMPORTANT CHALLENGES

Department of Resources, Energy and Tourism

Minister for Resources and Energy: The Hon. Martin Ferguson, AM MP

Secretary: Mr Drew Clarke

Geoscience Australia

Chief Executive Officer: Dr Chris Pigram



© Commonwealth of Australia (Geoscience Australia) 2011.

With the exception of the Commonwealth Coat of Arms and where otherwise noted, all material in this publication is provided under a Creative Commons Attribution 3.0 Australia Licence (<http://creativecommons.org/licenses/by/3.0/au/>)

Geoscience Australia has tried to make the information in this product as accurate as possible. However, it does not guarantee that the information is totally accurate or complete. Therefore, you should not solely rely on this information when making a commercial decision.

GeoCat # 72582

AnzlicID # ANZCW0703014875

Dataset # 14875

Bibliographic reference: R.C. Brodie and M.T. Costelloe 2011. Kombolgie VTEM™ AEM Survey: Inversion Report, Geoscience Australia internal report.

Web download URL:

https://www.ga.gov.au/products/servlet/controller?event=GEOCAT_DETAILS&catno=72582

Contents

Contents.....	3
Executive Summary.....	4
1 Introduction.....	5
1.1 Background.....	5
1.2 Previously released data	6
2 Kombolgie AEM data	8
2.1 System configuration.....	8
2.2 Data processing.....	10
2.3 Transmitter loop height	11
2.4 Waveform	11
2.5 Noise estimates	14
3 Layered earth inversion.....	17
3.1 Background on the GA layered earth inversion	17
3.2 Algorithm outline	18
3.2.1 Conductivity model parameterization	19
3.2.2 Reference model.....	20
3.2.3 Data misfit	21
3.3 Products	21
3.3.1 Layer conductivities	21
3.3.2 Depth slices	21
3.3.3 Elevation slices.....	21
3.3.4 Depth of investigation	22
3.3.5 Georeferenced conductivity sections.....	22
3.3.6 Multiplots	23
3.3.7 Gridding procedures	23
4 Qualifying remarks	24
4.1 Conductive areas of the Kombolgie dataset	24
4.2 Resistive areas of the Kombolgie dataset.....	27
4.3 Deep conductor in resistive areas	28
4.4 Shallow conductor in resistive areas	31
Acknowledgements	33
References	34
Appendix A GA-LEI inversion algorithm	36
Appendix B VTEM™ system file	47
Appendix C Inversion control file	48
Appendix D Digital data package	50
Appendix E Point located data header file.....	52
Appendix F Datum and projection	57

Executive Summary

Data acquired as part of the Kombolgie VTEM™ Airborne Electromagnetic Survey have been inverted using a layered earth inversion algorithm. Interpretation products have been derived from the inversion results. The inversion results and derived products have been released by Geoscience Australia as a digital data package.

The survey was funded under the Australian Government's Onshore Energy Security Program, and was managed and interpreted by Geoscience Australia's Airborne Electromagnetic Acquisition and Interpretation Project. The Kombolgie survey area, in the Pine Creek Orogen of the Northern Territory, covered sections of the Cobourg Peninsula, Junction Bay, Alligator River, Milingimbi, Mount Evelyn, Katherine, and Urapunga 1:250 000 map sheets. It collected a total of 8 800 line km and covered area of 32 000 km². The data were acquired under contract by Geotech Airborne Pty. Ltd. using its VTEM™ helicopter-borne electromagnetic system.

The inversions were carried out using the GA-LEI layered-earth inversion software developed at Geoscience Australia. Products include the layer conductivities, depth and elevation slices, and sections. The products are in digital form in both point-located and gridded formats. It is advised that interpreters carefully read these accompanying release notes which contain important qualifying remarks on the inversion results, data misfits, non-uniqueness and comparisons with EM Flow™ results. They are available for download from the Geoscience Australia website.

1 Introduction

1.1 Background

Airborne Electromagnetic (AEM) surveys are commonly used to map the electrical conductivity of the subsurface over large spatial areas. As an AEM system flies over the ground it carries a transmitter loop through which a time-varying current is passed, thereby inducing eddy (secondary) currents to flow in any electrically conductive subsurface material. These eddy currents may be detected via the voltage that they induce in receiver coils that are towed by the aircraft. Since the amount of current that flows in the subsurface is related to its conductivity, analysis of the received signals allows estimates of the conductivity to be made. The depth to which the signals can be used to map conductivity depends on the system configuration and the subsurface conductivity (Smith, 2001, Lane et al, 2004).

The Pine Creek AEM Survey is one of three regional AEM surveys undertaken as part of the Onshore Energy Security Program (OESP) at Geoscience Australia (GA). The survey area, located in the Pine Creek Orogen of the Northern Territory (Figure 1), covered sections of the Pine Creek, Cape Scott, Port Keats, Fergusson River, Mount Evelyn, Katherine, Alligator River, Darwin, Fog Bay, Cobourg Peninsula, Junction Bay and Milingimbi 1:250 000 map sheets (Costelloe et al., 2009). A total of 29 900 line kilometres of data were acquired along broadly-spaced flight lines (up to 5 km spacing).

The survey area was comprised of the Woolner Granite, Rum Jungle and Kombolgie sub areas. Fugro Airborne Surveys were contracted to fly the Woolner Granite and Rum Jungle areas using its fixed-wing TEMPEST™ system during 2008-2009. Geotech Airborne Pty. Ltd. (Geotech) were contracted to fly the Kombolgie area using its helicopter-borne VTEM™ system during 2008. Section 1.2 outlines the Pine Creek data and derived products that have previously been released by GA.

This report contains discussion on the inversion of the Kombolgie VTEM™ data to generate layered earth conductivity models. The Kombolgie survey covers a total of 8 800 line km and an area of 32 000 km². It was flown with 5 km line spacing. Internal to the regional block, one GA infill block was flown at 1.67 km line spacing. Two internal blocks and one external block, which were funded by subscriber companies, were also flown.

This report describes the inversion algorithm, qualification on the inversion models, the derived products and a digital data package, of which this report is one part. The digital data package contains conductivity information as layer conductivities, depth slices, elevation slices, conductance and cross section. They are presented in point located, gridded, and graphical formats.

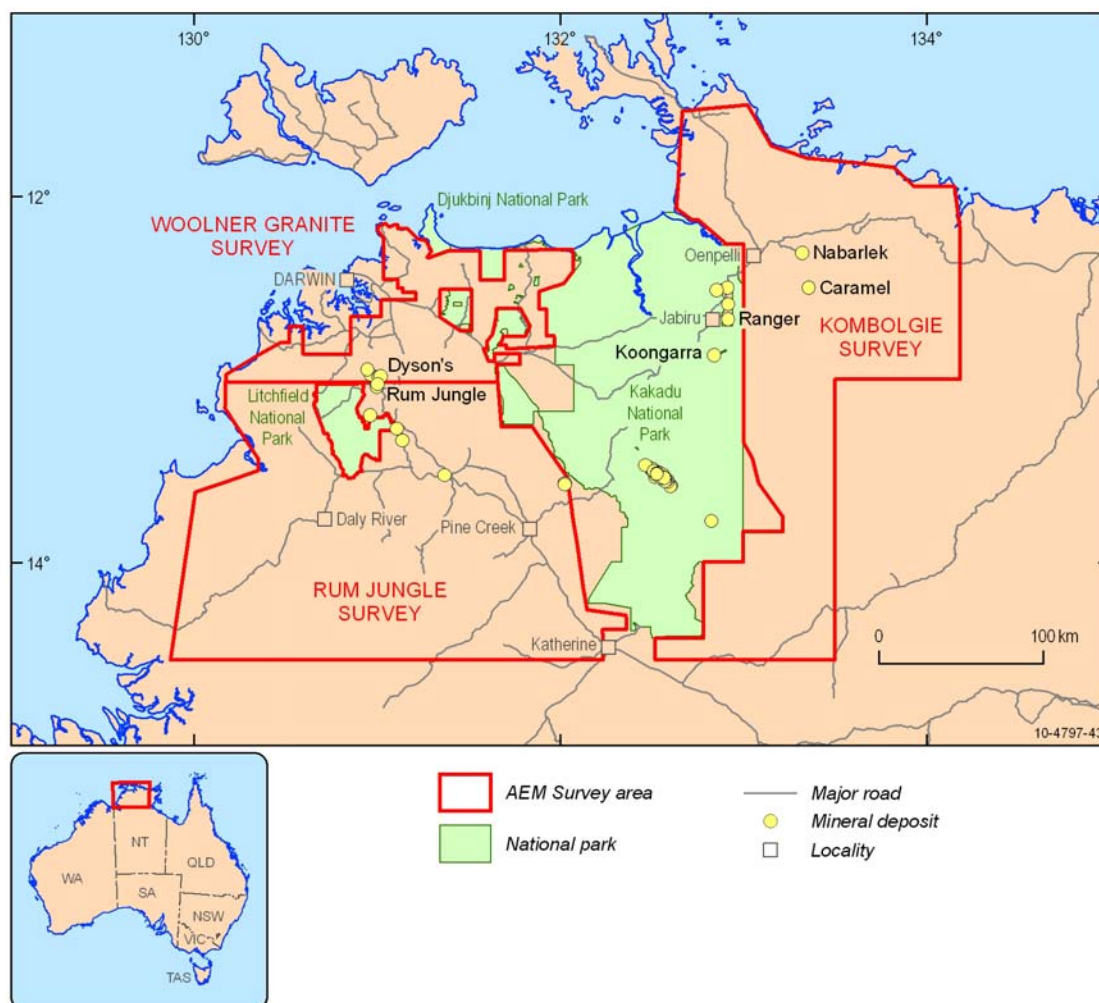


Figure 1: Locality map of the Pine Creek AEM survey area showing the boundaries of the Rum Jungle, Woolner Granite and Kombolgie sub areas.

1.2 Previously released data

Several Pine Creek AEM Survey datasets and reports have previously been released by GA. These data are available from the GA Sales Centre and are also available by free download from the GA web site using the links below.

Woolner Granite Area Phase-1 TEMPEST™ data package which included the acquisition and processing report, point located and gridded AEM response data, EM Flow™ conductivity models, and graphical multiplots.

https://www.ga.gov.au/products/servlet/controller?event=GEOCAT_DETAILS&catno=69228

Rum Jungle Area Phase-1 TEMPEST™ data package which included the acquisition and processing report, point located and gridded AEM response data, EM Flow™ conductivity models, and graphical multiplots.

https://www.ga.gov.au/products/servlet/controller?event=GEOCAT_DETAILS&catno=69230

Woolner and Rum Jungle Areas (excluding infill RJ7) Phase 2 TEMPEST™ inversion data package which included conductivity estimates produced by the GA layered earth inversion (GA-LEI) algorithm developed at GA, derived products and an inversion report.

https://www.ga.gov.au/products/servlet/controller?event=GEOCAT_DETAILS&catno=70584

Woolner and Rum Jungle Areas (infill RJ7 only) Phase 2 TEMPEST™ inversion data package which included conductivity estimates produced by the GA layered earth inversion (GA-LEI) algorithm developed at GA, derived products and an inversion report.

https://www.ga.gov.au/products/servlet/controller?event=GEOCAT_DETAILS&catno=71350

Kombolgie Area (excluding infill areas K1, K2 and K3) Phase-1 VTEM™ data package which included the acquisition and processing report, point located and gridded AEM response data, EM Flow™ conductivity models, and graphical multiplots. Due to download limitations, the point located data are only available from the GA Sales Centre on DVD.

https://www.ga.gov.au/products/servlet/controller?event=GEOCAT_DETAILS&catno=69230

Kombolgie Area (including infill areas K1, K2 and K3) Phase-1 VTEM™ data package which included the acquisition and processing report, point located and gridded AEM response data, EM Flow™ conductivity models, and graphical multiplots. Due to download limitations, this dataset is only available from the GA Sales Centre on DVD.

https://www.ga.gov.au/products/servlet/controller?event=GEOCAT_DETAILS&catno=71372

Kombolgie Area Phase 2 VTEM™ revised EM Flow™ conductivity estimates to 2 km depth conductivity estimates generated using a research version of EM Flow™.

https://www.ga.gov.au/products/servlet/controller?event=GEOCAT_DETAILS&catno=71371

Costelloe and Brodie (2011) have also reported on the above package and it is available from the link below.

http://www.publish.csiro.au/?act=view_file&file_id=PVv2011n150p29.pdf

A comprehensive report (Craig, 2011) which provides background to the surveys and their geological interpretation is to be released in late July 2011 and will be downloadable from the link below.

https://www.ga.gov.au/products/servlet/controller?event=GEOCAT_DETAILS&catno=71854

2 Kombolgie AEM data

2.1 System configuration

The Kombolgie survey area was flown by Geotech using the VTEM™ AEM System (Figure 2). The system was installed on an AS 350 B3 helicopter, registration VH-IPW. The survey logistics report (Carter et al., 2009) details the system specifications, as it was configured for the Kombolgie survey, and additional information on survey operations, data processing and the delivered data.

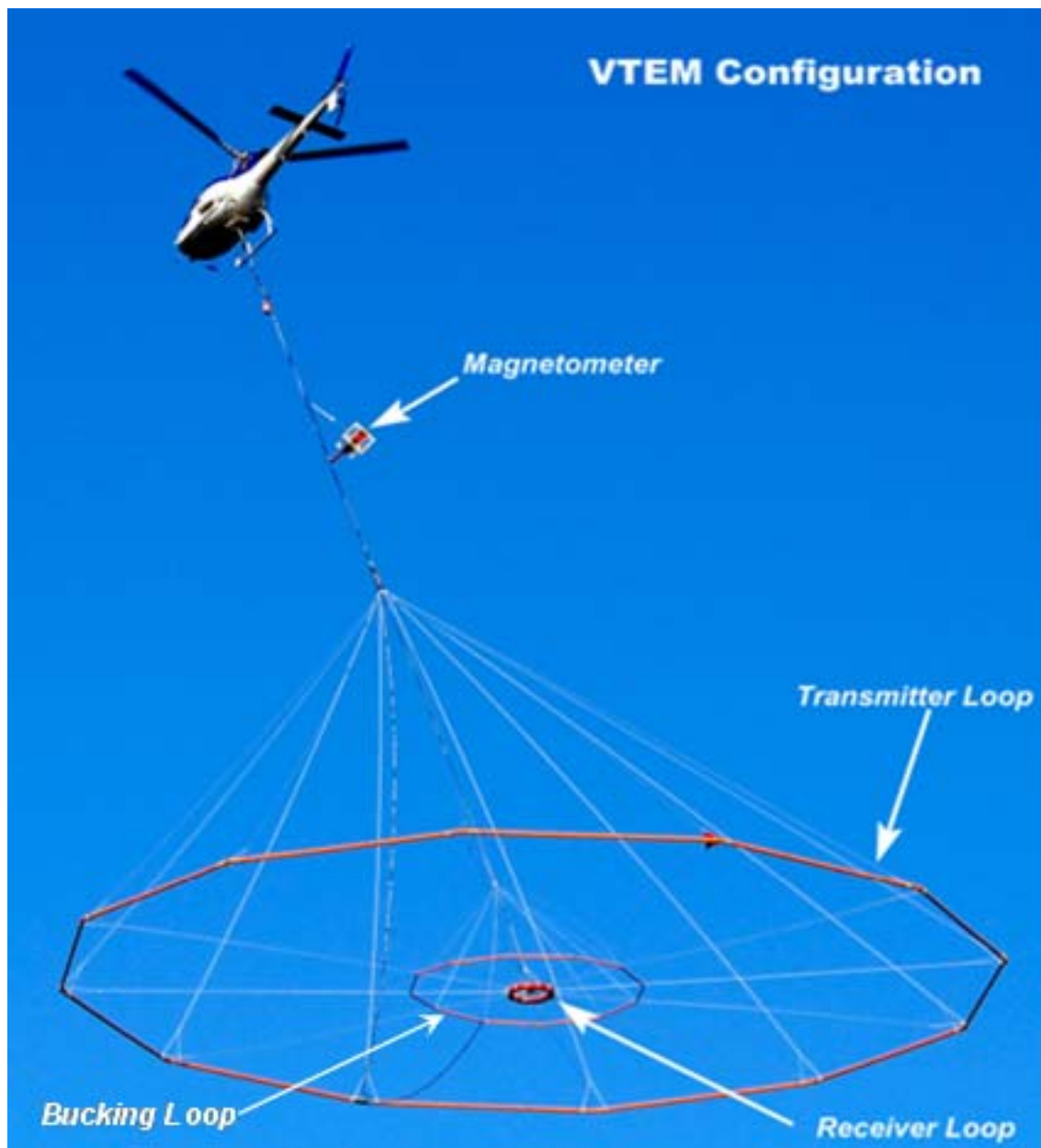


Figure 2: Photograph of VTEM™ in flight (modified from Carter et al., 2009).

Table 1: VTEM™ receiver sampling scheme.

Array Index	Window Number	Centre Time (μs)	Start Time (μs)	End Time (μs)	Width (μs)
1					
2					
3					
4					
5					
6	1	62.50	57.29	67.71	10.42
7	2	72.90	67.69	78.11	10.42
8	3	83.30	78.09	88.51	10.42
9	4	99.00	88.59	109.41	20.82
10	5	119.80	109.39	130.21	20.82
11	6	140.60	130.19	151.01	20.82
12	7	166.70	151.09	182.31	31.22
13	8	197.90	182.29	213.51	31.22
14	9	234.40	213.59	255.21	41.62
15	10	281.25	255.19	307.31	52.12
16	11	338.55	307.29	369.81	62.52
17	12	406.25	369.79	442.71	72.92
18	13	484.35	442.69	526.01	83.32
19	14	572.95	526.09	619.81	93.72
20	15	682.30	619.79	744.81	125.02
21	16	817.70	744.79	890.61	145.82
22	17	973.95	890.59	1057.31	166.72
23	18	1151.05	1057.29	1244.81	187.52
24	19	1369.80	1244.79	1494.81	250.02
25	20	1640.65	1494.79	1786.51	291.72
26	21	1953.15	1786.49	2119.81	333.32
27	22	2307.30	2119.79	2494.81	375.02
28	23	2744.80	2494.79	2994.81	500.02
29	24	3286.45	2994.79	3578.11	583.32
30	25	3911.45	3578.09	4244.81	666.72
31	26	4619.80	4244.79	4994.81	750.02
32	27	5494.80	4994.79	5994.81	1000.02
33	28	6578.15	5994.79	7161.51	1166.72
34	29	7828.15	7161.49	8494.81	1333.32
35	30	9244.80	8494.79	9994.81	1500.02

Data from array indices 1-5 were not contractual deliverables.

Data from array indices 6-9 (windows 1-4) were not used in the inversions.

VTEM™ is a central loop design, with the receiver positioned at the centre of a 26.1 metre wide dodecahedron shaped transmitter loop that is towed below the helicopter. The transmitter produces a dipole moment up to 625,000 (turns×A×m²) at peak current.

The 25 Hz base frequency waveform is bipolar, having a 7.33 ms pulse-width, including the 1.33 ms turn-off ramp, and a 12.66 ms off-time.

Measurements are made during the off-time, when the secondary field resulting from eddy currents flowing in conductors in the ground are not dominated by the primary field. VTEM™ measures the voltage induced ($\propto dB/dt$) in the receiver coil at 96 kHz. B-Field data are obtained through real-time electronic integration of the dB/dt data, similar in concept to the process described by Smith and Annan (2000).

The 96 kHz receiver samples are windowed using a linear-tapered shaped filter. The time ranges are shown in Table 1. It is important to note that nominally 35 window positions are specified, but positions 1-5 were not deliverables for the Kombolgie survey contract. Additionally, we chose not to use the first four of the delivered windows (array indices 6-9) in the layered earth inversions. This was because these four windows were the most seriously impacted by parasitic capacitance effects (Macnae and Baron-Hay, 2010) which cause the transients to rise rather than decay at early time.

2.2 Data processing

Processing of the Kombolgie dataset was carried out by Geotech. Carter et al., (2009) describe the data processing steps and the various datasets that were delivered to GA. The list below broadly summarizes the processing steps applied.

1. Flight path recovery.
2. Parallax and lag corrections.
3. Altimeter corrections.
4. Digital elevation model calculation.
5. Transmitter loop height determination.
6. Windowing and electromagnetic data sferics rejection by non-linear filtering is understood to occur onboard the aircraft within the data acquisition system (generates 'raw' or Zsr data).
7. Electromagnetic compensation to account for high frequency fluctuations in the system geometry, particularly the transmitter loop shape (generates 'compensated' or Zsc data).
8. Electromagnetic data low-pass filtering consisting of a 4 samples or a 0.4 second non-linear filter followed by a linear smoothing filter of maximum width 20 samples.
9. Electromagnetic drift correction in which a piecewise linear interpolation of zero-levels, which were measured at high altitude two or three times per flight, are subtracted from the data. (generates 'filtered and drift corrected' or Zsf data).
10. Electromagnetic final levelling in which static level adjustments were applied to entire flight lines window data in order to remove corrugations observed in grids that are deemed to be attributed to system variations (generates 'final levelled' or Zsl data).

Geotech delivered four streams of electromagnetic data to GA; the (i) raw or Zsr data following Step 6, (ii) compensated or Zsc data following Step 7, (iii) filtered and drift

corrected or Z_{sc} data following Step 9, and (iv) final levelled or Z_{sl} data following Step 10. The raw Z_{sr} data are confidential under the terms of the contract between GA and Geotech, and hence have not been released by GA.

2.3 Transmitter loop height

The system was equipped with radar and laser altimeters, mounted on the helicopter, to monitor terrain clearance. The distance z_0 below the helicopter that the transmitter loop flies is subtracted from the altimeter data, taking lag and various offsets into account, to attain the transmitter loop height above the ground. Initially, Geotech estimated $z_0=37$ using knowledge of the cable length and angles measured from photographs of the system in flight. GA's quality control of the processed data suggested that the estimated z_0 may have been incorrect. This was because of discrepancies between data measured over seawater of known depth and the corresponding forward models (Brodie, 2009a).

Subsequent inversion and modelling (Brodie, 2009b) and a revision of photographs by Geotech (2009a), suggested that it was probable the loop was flying in the vicinity of 5.2 m higher ($z_0=31.8$) to 9 m ($z_0=28$) higher than Geotech originally anticipated and delivered with the initial data. Following this, Geotech then mounted GPS units on the transmitter loop and flew calibration tests off Western Australia in April 2009 (Geotech, 2009b). The results showed that the transmitter loop was likely to have been flying 6.8 m higher ($z_0=30.2$) than was initially anticipated. This amounted to the tow cable being at 44° from the vertical on average.

The Kombolgie dataset was then reprocessed by Geotech to take into account the new information. It was assumed that the parameters determined in the calibration flights in Western Australia were representative of the Kombolgie survey and the 44° tow cable angle was used in the transmitter loop height calculations for the entire Kombolgie dataset. These transmitter loop height estimates have been included in previous Kombolgie data releases and have also been used for the layered earth inversions. It should be noted though, that the constant tow cable angle estimate does not account for variations in the transmitter loop position due to variations in aircraft and wind speed.

2.4 Waveform

On typically two to three occasions per flight, the system was flown to a height of 1100 m above ground level to make zero-level measurements to be used in drift corrections. At altitude voltage waveform files were also recorded and supplied to GA with the delivered dataset. A total of 272 waveform files were acquired. GA understands that the voltage waveforms are not measured with the receiver coil circuitry itself, but with a device that monitors the time derivative of the transmitter current. For forward modelling an inversion we had to choose a representative waveform.

We assembled all 272 recorded receiver waveforms that were acquired at high altitude during the survey and subsequently delivered by the contractor. They were: (i) time-synchronised according to the time-zero definition (i.e., midway between the two samples on the off-ramp over which the voltage falls to half its peak negative

amplitude); (ii) normalized to unit negative voltage; and, (iii) then sorted according to the voltage at time-zero.

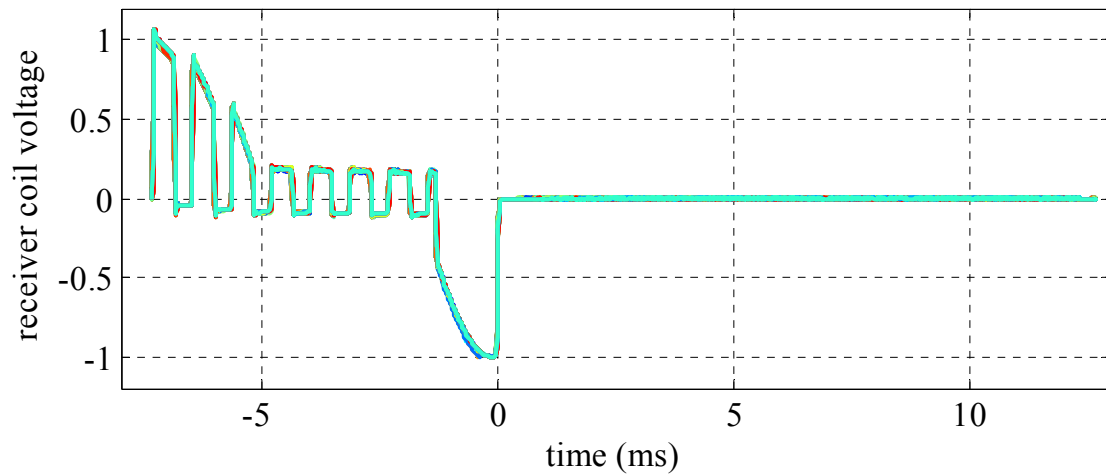


Figure 3: All 272 of the recorded voltage waveforms after time-synchronisation and normalization.

We then selected the most representative waveform to be the middle of the sorted waveforms, which might also be described as a median shaped waveform for the survey. This was the waveform from high altitude line 70603 flown during flight number 60. Figure 3 shows all 272 of the voltage waveforms after time-synchronisation and normalization. Figure 4 shows the same information in detail around the turn-off ramp, and with the chosen representative waveform from high altitude line 70603 plotted in a thick black line. We could have simply chosen to average the time-synchronised and normalized waveforms to get an average waveform. However, we chose not to do this as it would have amounted to smoothing of the waveforms, which was not desired.

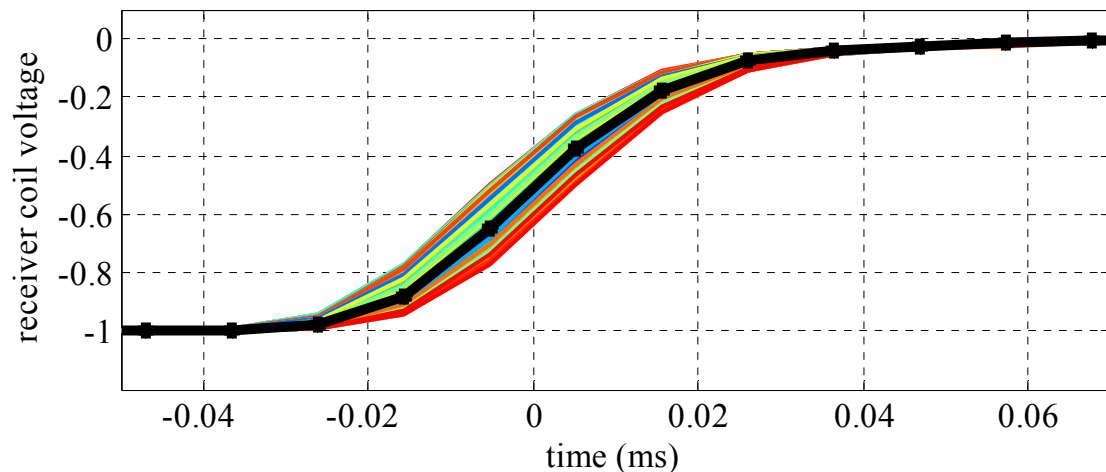


Figure 4: The details of the waveforms in Figure 3 around the turn-off ramp and with the selected representative waveform highlighted in black.

After selecting the ‘median’ survey waveform, we applied a filter to it using a program and filter parameters supplied to GA by Professor James Macnae. The filter simulates the effect of the receiver-side electronics and has the effect of slightly delaying and smoothing the ‘transmitter-measured’ receiver waveform so that it more closely represents a true ‘receiver-measured’ waveform that is actually required. The output filtered waveform was then zeroed after 0.286 ms (part way through window 10) where the voltage falls to its noise level at approximately 10^{-4} of its peak amplitude. The effect of the waveform filter is shown in **Figure 5**, where the representative waveform (black) was filtered to produce a slightly delayed waveform (red).

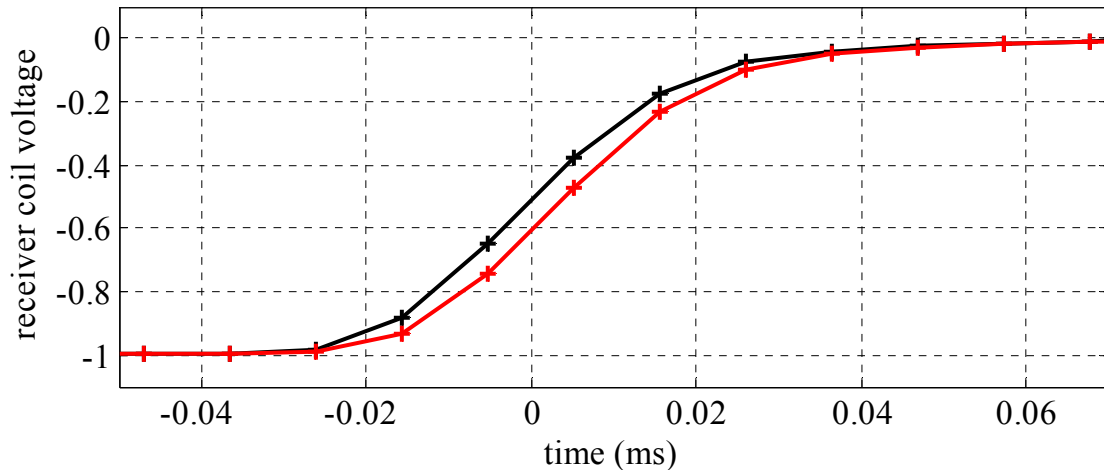


Figure 5: The representative transmitter-side measured waveform (black) was filtered to account for receiver side electronics to produce a slightly delayed waveform (red).

The filtered receiver waveform was then transformed by Fast Fourier Transform (FFT) to generate an equivalent transmitter current waveform for use in the forward modelling and inversion. Figure 6 shows the resultant transmitter current waveform and Figure 7 shows the details around time-zero. Also shown in Figure 7, in black, is the transmitter current waveform that corresponds to an unfiltered version of the receiver waveform (i.e., the black receiver waveform shown in **Figure 5**).

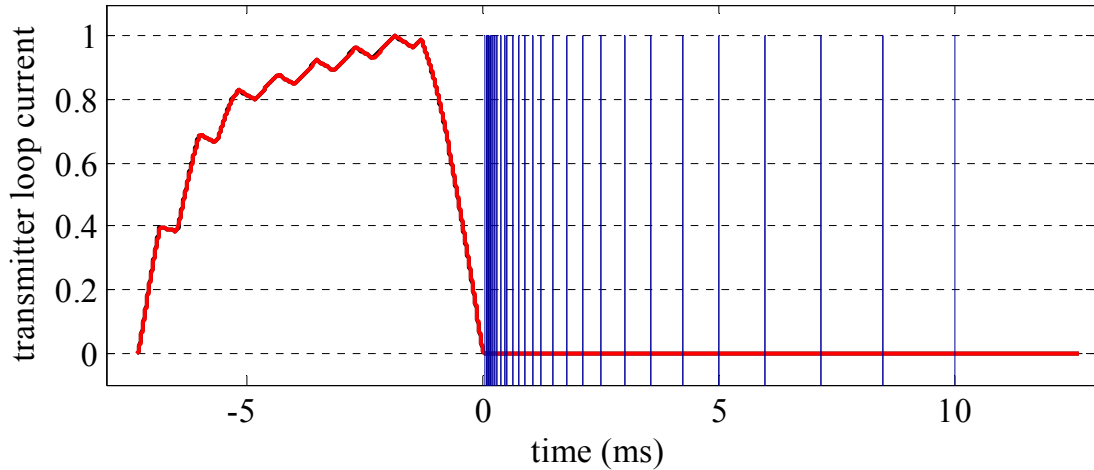


Figure 6: The normalized transmitter current used for forward modelling and inversion. The thirty receiver window positions are shown in blue.

The normalized transmitter current waveform used in the inversion is available in the accompanying digital data package along with the corresponding receiver voltage waveform (cf. VTEM.cfm in Appendix B and Appendix D). The waveform is digitised at 96 kHz, normalized to 1 A maximum current and the time reference is the same as the receiver window times shown in Table 1.

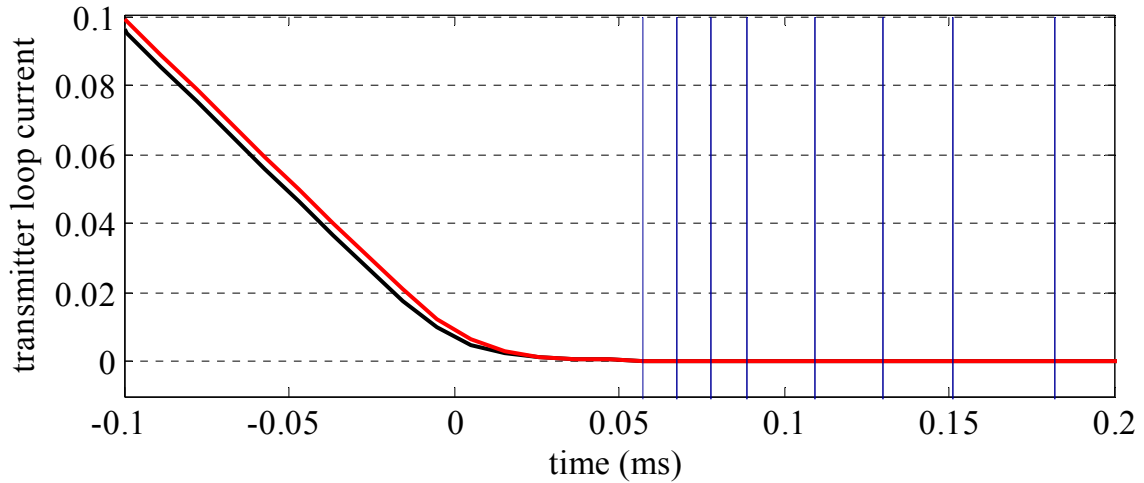


Figure 7: Details around time-zero of the normalized transmitter current used for forward modelling and inversion (red). The black transmitter waveform corresponds to the unfiltered receiver waveform. The first seven receiver window positions are shown in blue.

2.5 Noise estimates

We used the method developed by Green and Lane (2003) to estimate noise levels in the data that were required in the inversion algorithm. Repeat line data were used to estimate multiplicative (or relative) noise. Unfortunately most of the repeat lines were situated over resistive ground where the signal level is low and consequently the

algorithm does not perform adequately. However we had one set of two repeat lines over conductive ground from which we estimated a relative error of 3.6% of the response.

High altitude data were used to determine the additive component of the noise. Each of the thin grey curves on Figure 8 represents the standard deviations, in each time window of the filtered and drift corrected (Zsf) data, calculated over the length of each high altitude calibration line in the survey. To attain a representative additive noise level we take the median value, in each window, of all the individual high altitude line Zsf standard deviations. This is represented as a thick blue curve on Figure 8. The red curve represents the same quantity except it was calculated for the compensated Zsc data that had not been filtered or drift corrected. It demonstrates the noise reduction of over an order of magnitude due to the filtering.

The black curve on Figure 8 is the same except that a linear trend was removed from the Zsf data prior to calculating the standard deviations. This lowered the early time standard deviations because significant trends (drifts) had been observed in the early time high altitude data. It is not clear what the reason is for these drifts over calibration lines of the order of 1 minute in duration. However, we have used the median trend-removed high altitude line Zsf standard deviations (black curve) as our estimate of the additive noise in the inversion. These noise values are listed in the inversion control file Appendix C adjacent the tag *ZAdditiveNoise*.

We did not use values calculated from final levelled Zsl high altitude data, which we actually inverted, because those data are undefined in the Zsl data since levelling correction are not applied to high altitude data.

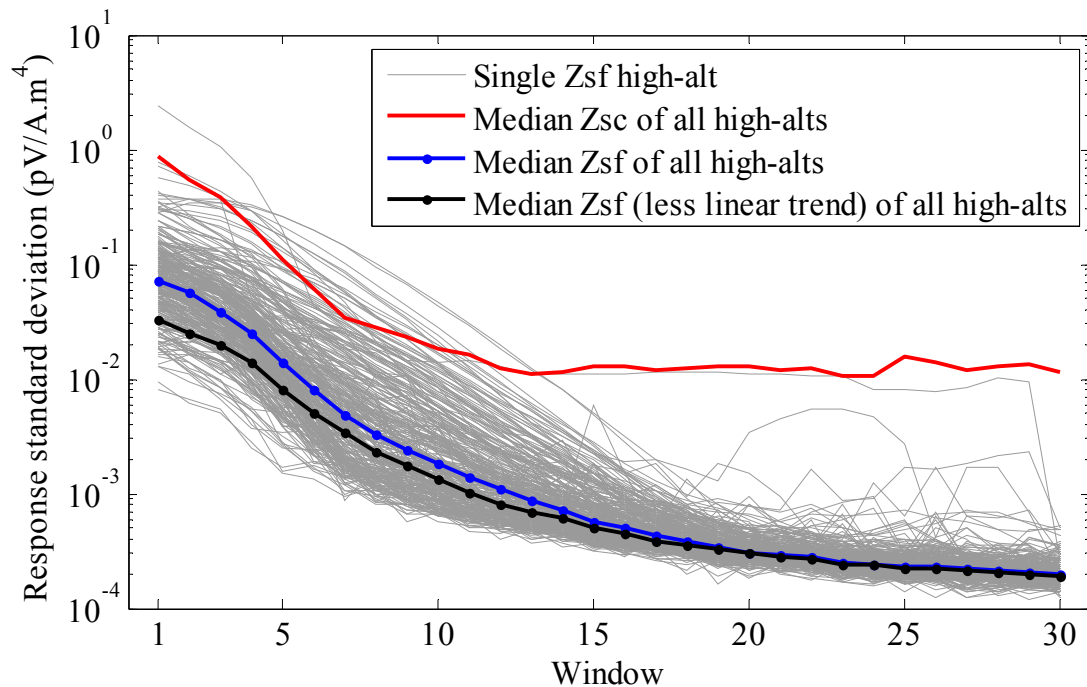


Figure 8: Standard deviations calculated from high altitude data which were used as additive noise estimates in the inversion.

We also analysed the means of each of the high altitude lines to attain an estimate of possible bias error in the data. The results are shown in Figure 9, which is linearly scaled, and Figure 10 which is logarithmically scaled. The absolute value of the means is plotted in the logarithmic figure so that the negative biases can be shown. It can be seen that there are significant biases, particularly in the early time windows. Furthermore there are large variations in the biases.

The reason for these biases is thought to be due to parasitic capacitance effects (Macnae and Baron-Hay, 2010). Parasitic capacitance results in imperfect bucking-out of the primary field. In the Kombolgie dataset it typically results in transients, including those recorded at survey altitude that rise rather than decay at early time. Because of this we have not used the first four windows in the inversion of the Kombolgie data.

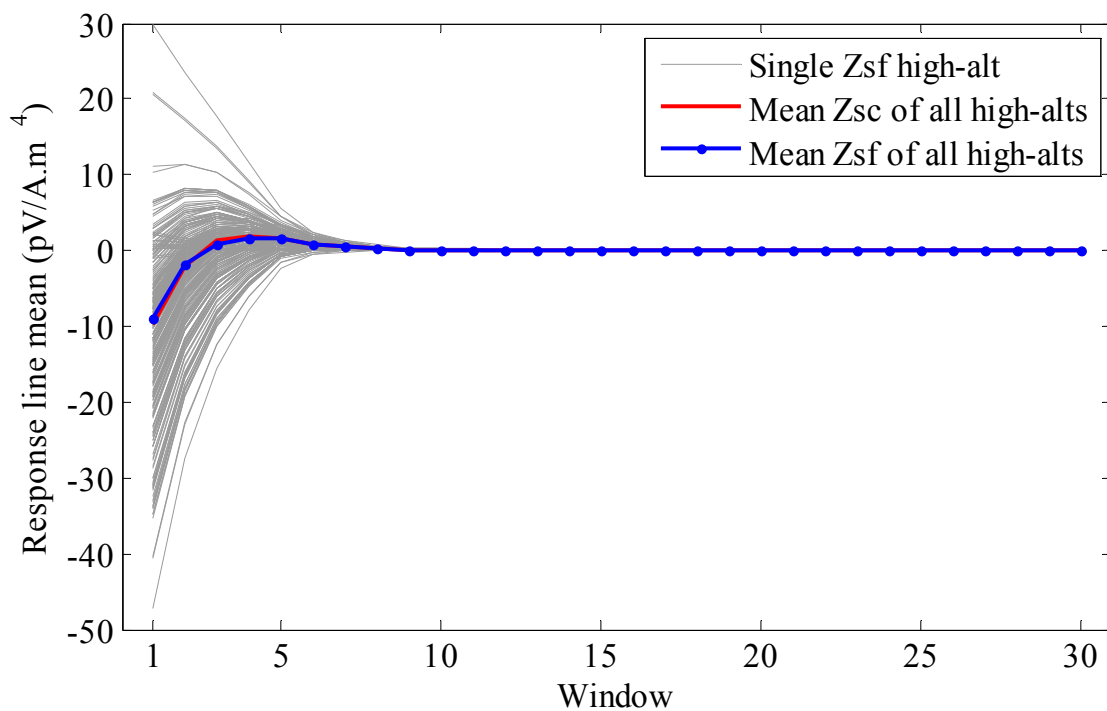


Figure 9: Linear scaled plot of the means of high altitude lines.

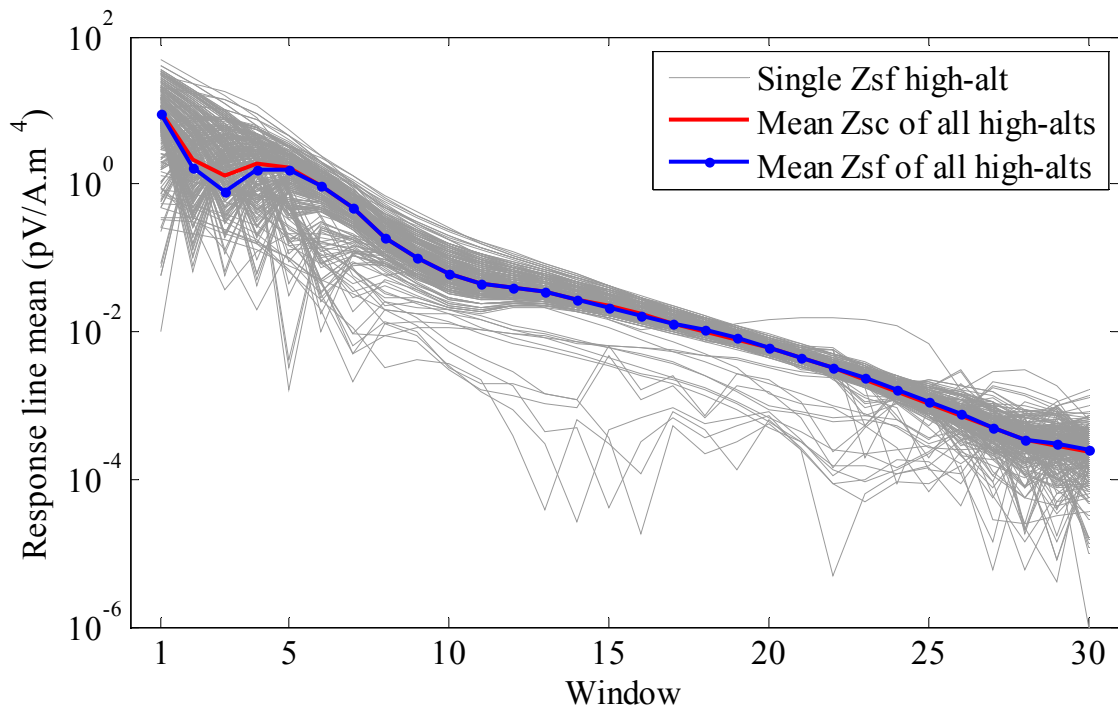


Figure 10: Logarithmic scaled plot of the absolute value of the means of high altitude lines.

3 Layered earth inversion

3.1 Background on the GA layered earth inversion

Conversion of the non-linear electromagnetic response data into estimates of subsurface conductivity allows for much easier and more accurate integration with independent subsurface information and facilitates better interpretation. The conversion can use either approximate transformation methods or geophysical inversion, both of which produce model-dependent conductivity estimates.

The Phase-1 data release of Kombolgie AEM data included conductivity predictions produced by Geotech from the industry standard EM Flow™ algorithm (Macnae et al., 1998; Stolz and Macnae, 1998). Later, GA generated and released further EM Flow™ conductivity estimates, extending the depth of estimates to 2 000 m, with a more recent research version of the software (Costelloe and Brodie, 2011). EM Flow™ is a fast approximate transformation method based on the concept that the response of a quasi-layered earth can be approximately represented by a mirror image of the transmitter dipole that recedes below the surface and expands with delay-time. By determining the vertical depth distribution of the mirror image dipoles a quasi-layered estimate of the subsurface conductivity can be estimated.

The GA Layered Earth Inversion (GA-LEI) algorithm was originally developed to overcome shortcomings in the application of EM Flow™ to data from fixed-wing towed-bird AEM systems like TEMPEST™. It was designed to solve for, in addition to

the conductivity structure, three system geometry parameters which could not be measured in fixed-wing systems that had to be assumed or estimated in the data processing. Errors in those estimates led to incorrect primary field removal, and consequently prevented both X- and Z- components being able to be simultaneously fitted in EM Flow™ or inversion algorithms.

Previous work at GA, in which downhole conductivity log data were compared to conductivity estimates (e.g., Lane et al, 2004; Reid and Brodie 2006; Brodie and Fisher, 2008), has shown that improvements on the standard EM Flow™ conductivity estimates can be made using the GA-LEI algorithm. However, the same issues of system geometry estimation do not apply to the central loop helicopter AEM systems like VTEM™ that acquired the Kombolgie data.

3.2 Algorithm outline

A complete technical description of the GA-LEI is provided in Appendix A. Note that the appendix was written with the inversion of TEMPEST™ fixed-wing towed-bird AEM system data in mind. Therefore some of the aspects, relating to for example, solving for transmitter-receiver offsets, X-component data, and reinstatement of the total field, are not relevant to Kombolgie VTEM™ data. Nevertheless the underlying algorithm is identical. A less technical description of its application to the Kombolgie VTEM™ dataset is provided below.

The GA-LEI is a 1D “sample-by-sample” inversion in which each of the airborne samples, acquired at approximately 12 m intervals along a flight line, are inverted independently of their neighbours. The inversion of each individual sample involves the estimation of a 1D layered earth conductivity structure (Figure 11) that is consistent with the data. A 1D layered earth conductivity structure means that the earth is considered to be a series of horizontal layers stacked in layer-cake fashion. Each layer extends to infinity in the horizontal direction and the conductivity within each layer is constant.

Since the data are non-linear with respect to the model parameters, an iterative inversion technique is used. Starting from an initial model, the layer conductivities and system geometry parameters are iteratively updated until the theoretical forward response of the model fits the measured data to within the noise levels of the data, or in other words, until a satisfactory data misfit (*cf.* Section 3.2.3) is achieved. We used noise levels as described in Section 2.5 in the inversion.

Because of non-uniqueness, the estimated conductivity model must be constrained. In the GA-LEI it is constrained to be vertically smooth and to be as close as possible to a reference conductivity model (*cf.* Section 3.2.2). The aim of these smoothness and reference model constraints is to ensure that the model is as simple as possible, and complex structure is only permitted where necessary, see for example Constable et al. (1987).

Once all individual samples are inverted they are compiled into a pseudo-3D model by ‘stitching’ the 1D models together.

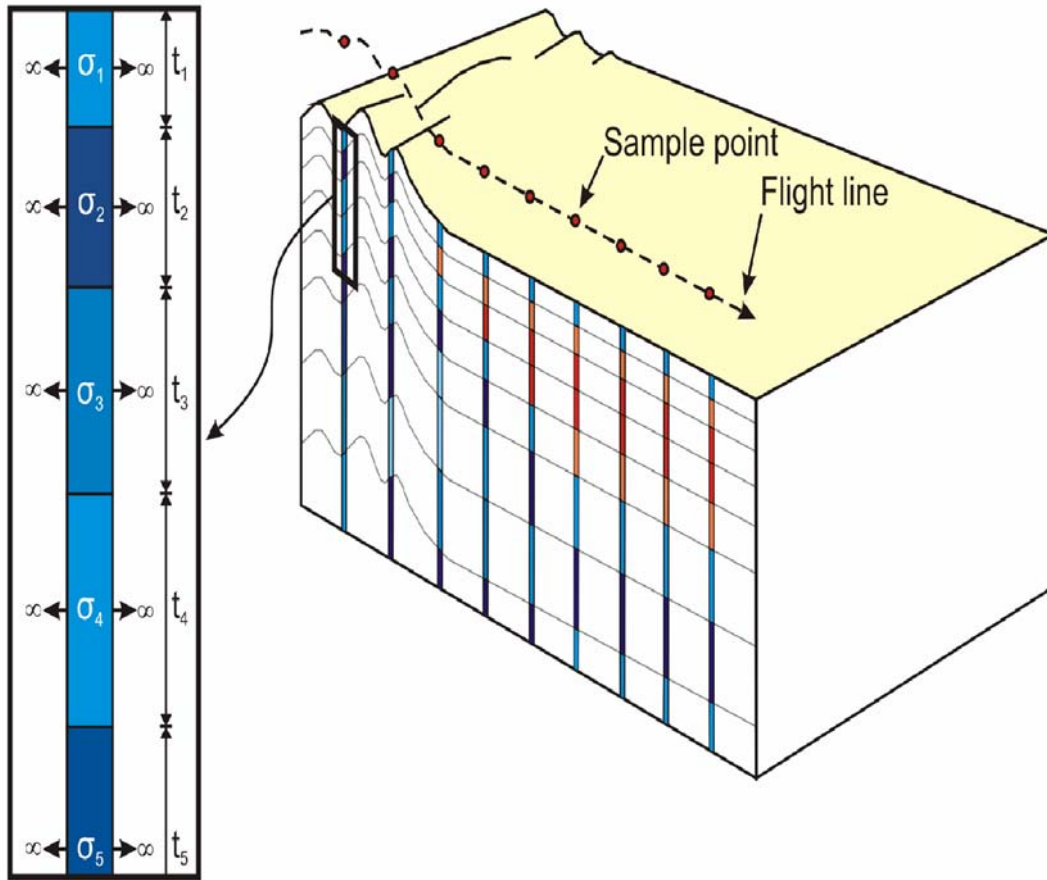


Figure 11: Schematic diagram of 1D layered earth model used in the GA-LEI. The thickness of each layer (t_n) is fixed, but the conductivity (σ_n) is not fixed and can vary across the survey area.

3.2.1 Conductivity model parameterization

The subsurface was parameterized with 30 layers whose thicknesses were chosen and remained fixed throughout the inversion (i.e., they were not solved for). The layer thicknesses gradually increase from 12 m in the top layer of the model up to 173 m in the second deepest layer. The bottom layer was set to infinite thickness and thus represents a halfspace below all other layers. The parameters of each layer used in the GA-LEI are shown in Table 2.

Table 2: *GA-LEI model layer thicknesses and depths from surface.*

Layer	Thickness (m)	Depth top (m)	Depth bottom (m)
1	12.00	0.00	12.00
2	13.20	12.00	25.20
3	14.50	25.20	39.70
4	16.00	39.70	55.70
5	17.60	55.70	73.30
6	19.30	73.30	92.60
7	21.30	92.60	113.90
8	23.40	113.90	137.30
9	25.70	137.30	163.00
10	28.30	163.00	191.30
11	31.10	191.30	222.40
12	34.20	222.40	256.60
13	37.70	256.60	294.30
14	41.40	294.30	335.70
15	45.60	335.70	381.30
16	50.10	381.30	431.40
17	55.10	431.40	486.50
18	60.70	486.50	547.20
19	66.70	547.20	613.90
20	73.40	613.90	687.30
21	80.70	687.30	768.00
22	88.80	768.00	856.80
23	97.70	856.80	954.50
24	107.50	954.50	1062.00
25	118.20	1062.00	1180.20
26	130.00	1180.20	1310.20
27	143.00	1310.20	1453.20
28	157.30	1453.20	1610.50
29	173.10	1610.50	1783.60
30	∞	1783.60	∞

3.2.2 Reference model

In principle, conductivity logs can be used to create a detailed reference model that varies across the survey in order to constrain the inversion. In the survey, just 7 confidential conductivity logs from industry holes were available for use in the inversion. Since there were relatively few conductivity logs available over a large survey area, it was not feasible in this case to define a conductivity reference model that was spatially variable. Therefore the reference model used in this inversion is simply a half-space of homogeneous conductivity across the survey area. Since inductive conductivity logs are not sensitive to conductivity variations at the 0.001 S/m level they were not useful in defining a reference model in this extremely resistive terrain. We chose to use a conductivity reference value of 0.0001 S/m based on confidential

industry resistivity logs. The reference model was also used as the starting model for the iterative inversion.

3.2.3 Data misfit

The inversion would ideally converge until the data misfit (Φ_d) reaches a value of 1.0 (*cf.* Equation 9 in Appendix A). The data misfit is simply a measure of fit (agreement) between the forward response of the inversion model and the observed data. It is not a measure of confidence or certainty or uniqueness in the model parameters. In 1D geological environments it is usually possible to achieve a data misfit of 1.0 or close to 1.0. However, in geological environments with 2 or 3D geology, 1D inversions usually have a higher data misfit, reflecting the fact that a 1D model is insufficient to explain anomalies caused by the 2 or 3D geology.

3.3 Products

3.3.1 Layer conductivities

The conductivity of all 30 of the layers in the inversion is the fundamental output of the inversion program. Several other products are then derived from these layer conductivities. Layer conductivities are included in the digital data package (Appendix D) as point located line data and as grids.

Since the inversion actually solves for base ten logarithm of the layer conductivities, we grid the point located layer conductivity data in these units. We have found that this produces better quality grids than gridding in linear conductivity units. However the grids are provided in both logarithmic and non-logarithmic units. This also applies to the gridding of the derived depth and elevation slice data explained in the following sections. The procedures used for gridding are described in Section 3.3.7.

3.3.2 Depth slices

A conductivity depth slice is the average estimated conductivity over a given constant depth interval below the topographic surface. Depth slices are included in the digital data package (Appendix D) as point located line data and as grids.

A series of depth slices have been created between 0 and 2 000 m, with the slices becoming progressively thicker with depth. The depth slices are set to, 20 m thickness between 0 and 100 m depth, 50 m thickness between 100 and 500 m depth, 100 m thickness between 500 and 1 000 m depth, and 200 m thickness between 1 000 and 2 000 m depth. The increase in thickness with depth reflects the lower sensitivity of the inversion with depth.

3.3.3 Elevation slices

In contrast to the depth slices, the elevation slices present the same inversion results, but the slices are relative to the height above sea level rather than depth below ground surface. This is useful because it removes the complications that a rough topography may introduce into depth slice interpretation. Furthermore, elevation slices provide a

simpler means of importing the data into modelling and visualization packages. The drawback of using elevation slices over the entire survey is that, if there is a substantial altitude difference across the survey, a given elevation slice may display near-surface data from one corner of the survey area with much deeper data from other parts of the survey area.

Elevation slices were created for elevations from 2 000 m below sea level to 450 m above sea level at 50 m intervals. Elevation slices are included in the digital data package (Appendix D) as point located line data and as grids.

3.3.4 Depth of investigation

We calculated a depth of investigation (DOI) using a variation on the method of Christiansen and Auken (2010). This method is based on a parameter S_j , which is an expression of the total AEM response sensitivity to noise ratio. This method has the advantage of being completely data driven, since it does not consider a priori information or model constraints involved. It also normalises the sensitivity with respect to the noise in the data. The sensitivity parameter for the j th model layer S_j is defined as,

$$S_j = \sum_{i=1}^{N_D} \left| \frac{1}{d_i} \times \frac{1}{\log_e 10} \times J_{ij} \times \frac{1}{n_i} \right| = \sum_{i=1}^{N_D} \left| \frac{1}{d_i} \times \frac{1}{\log_e 10} \times \frac{\partial d_i}{\partial \log_{10}(\sigma_j)} \times \frac{1}{n_i} \right|,$$

where, d_i and n_i are the i th datum and its noise, N_d is the number of data, and σ_j is the j th layer conductivity. The term J_{ij} is the Jacobian or sensitivity matrix for the final model (cf. Equation 19 of Appendix A). Thus each element of the vector S is the sensitivity for each conductivity parameter summed over all the data. The expression is a variation on the one given by Christiansen and Auken (2010) because: we do not invert the logarithm of the data; we invert for the base-10 rather than natural-logarithm of the layer conductivities; and our data may be negative so we use the absolute value.

We then calculate the cumulative sum T_k of the sensitivities, from the bottom layer (N_L th) to the k th layer,

$$T_k = \sum_{j=N_L}^k S_j,$$

which gives a measure of sensitivity that decreases uniformly with depth. We use Christiansen and Auken's value of 0.8 as the threshold to set the DOI (i.e. the deepest layer k such that $T_k < 0.8$). This threshold is a somewhat arbitrary value, chosen based on experimentation with a range of test cases.

The depth of investigation is plotted on the goereferenced conductivity sections and multiplots. It is not available in the digital data.

3.3.5 Georeferenced conductivity sections

Conductivity-depth sections depicting the GA-LEI inversion results along each flight line are provided as georeferenced conductivity section images. They are included as a

convenient way to overlie inversion results into GIS software. Each of the survey flight lines has a JPEG image file (.jpg) depicting the conductivity-depth section of the GA-LEI results along the flight line. Each image file has an associated JPEG world file (.jgw) that spatially locates or georeferences the image file (Table 3).

The images are georeferenced such that the average topographic height on the section will display approximately coincident with the line-of-best-fit of the flight line when loaded into a GIS package. They were produced with a vertical exaggeration of 2.5. A colour scale bar for the sections is included in the digital data package.

Table 3: Example contents of a JPEG world file from line 10010

Parameter	Value
x scale (per pixel)	8.449337
rotation about y axis	-0.000202
rotation about x axis	-0.000202
y scale (per pixel)	-8.449337
x reference point	244650.705562
y reference point	8722983.469149

3.3.6 Multiplots

The multiplots show the conductivity depth section for each flight line along with a number of auxiliary panels showing information such as the system geometry. They are provided as Portable Document Format (.pdf) files. Table 4 details the information that is shown in each panel, from top to bottom, of the multiplot.

Table 4: Description of each panel of the multiplots

Φ_d	Data misfit of the inversion, the optimal misfit is 1.0.
Data	Z-component window data profiles logarithmically scaled.
TX Height	Transmitter height in metres.
Geology	Image strip showing 1:1M surface geology
Elevation	Gradient enhanced surface elevation image strip
Satellite imagery	Satellite image strip
GA-LEI Conductivity section	Conductivity-depth section image with conductivity colour bar in (S/m).
EM Flow™ Conductivity section	Conductivity-depth section image with conductivity colour bar in (S/m).
Easting	Labelled every 2000m
Northing	Labelled every 5000m

3.3.7 Gridding procedures

The AEM inversion results were gridded using Intrepid™ software to a grid cell size of 185 m. They are stored in binary files as ER Mapper™ single band IEEE 4 Byte Real

data types. A comprehensive ER Mapper™ header (.ers) file is associated with each grid file, which describes the data type and the coordinate system used to geographically position the grid. Gridded data are stored in a projected coordinate system only, in this case Universal Transverse Mercator (metric) coordinates of the Map Grid of Australia Zone 53 using the Geodetic Datum of Australia 1994. Technical details of the projection used are given in Appendix F.

In the Kombolgie survey the line spacing is as wide as 5 km. It was deemed more appropriate to not interpolate data across 5 km to reduce artefacts that obscure the structure evident in the data in some areas. In this area the data appears as coloured stripes with null values in between.

4 Qualifying remarks

The purpose of this section is to make interpreters aware of the capabilities and uncertainties to be taken into account when interpreting the conductivity estimates generated from the Kombolgie Airborne Electromagnetic (AEM) dataset. All conductivity estimates from AEM surveys are uncertain and should be interpreted with this in mind. The uncertainty stems from the level of noise in the dataset as well as the non-uniqueness of conductivity transformations and AEM inversions.

4.1 Conductive areas of the Kombolgie dataset

In conductive areas of the Kombolgie dataset the AEM response (signal) is large and thus there is a high signal-to-noise ratio. In these areas the uncertainty stems mainly from the non-uniqueness, which is most pronounced below the depth of investigation.

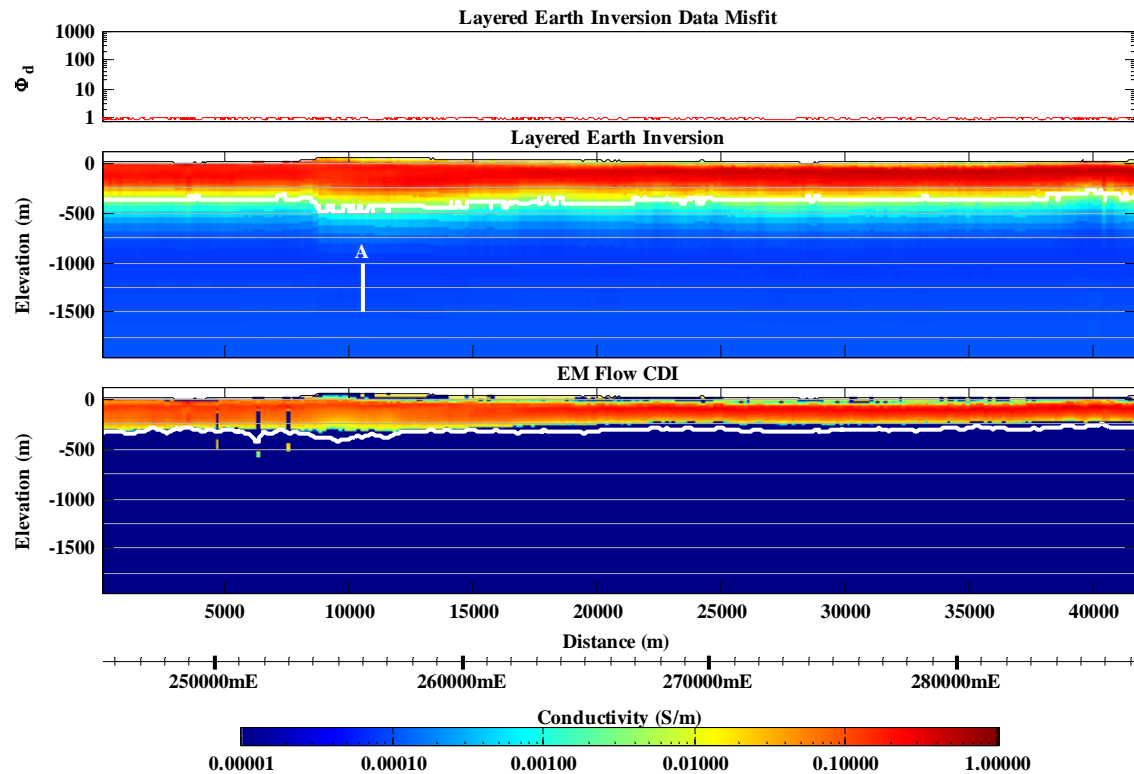


Figure 12: GA-LEI and EM Flow™ conductivity sections from a conductive part (Line 10010) of the Kombolgie survey area.

In the conductive areas the AEM data have been able to be successfully fitted, to within the ascribed noise levels, using Geoscience Australia's layered earth inversion algorithm (GA-LEI). Figure 12 shows an example GA-LEI and the corresponding EM Flow™ CDI conductivity section for a conductive portion (Line 10010) of the survey area. The white lines on each section are the estimated depths of investigation. Note from the top panel that the GA-LEI data misfit (Φ_d) is at the value of 1.0 for the entire line indicating a good data fit. In this case the GA-LEI and CDI show qualitatively similar results.

Figure 13 shows the details of the data and fitted model at the position 'A' marked on the conductivity sections in Figure 12. The left hand panel shows, in order of VTEM™ data processing steps, the filtered (blue), filtered and drift corrected (green) and final levelled (black) data transients. The forward models of the GA-LEI (magenta) and EM Flow™ CDI (red) conductivity models are shown in the same colours on the right hand panel. Although difficult to see in this particular case, because they are small, the estimated data error (± 1 standard deviation) bars are also shown on the final levelled data (black). The GA-LEI and EM Flow™ CDI were both generated using the final levelled data as input.

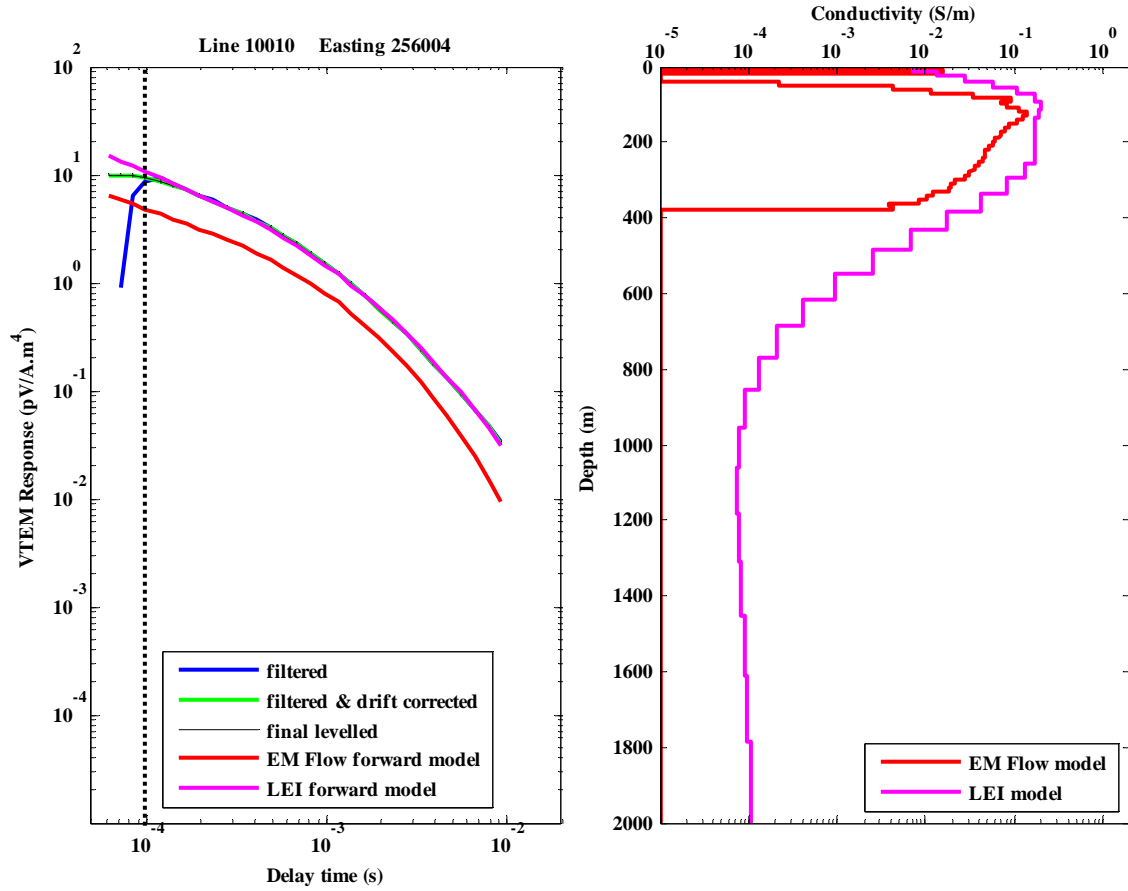


Figure 13: VTEM™ data (left) at the sample located at 'A' on Figure 12 and the corresponding GA-LEI and EM Flow™ CDI conductivity models (right).

The first four windows (i.e., left of the vertical dotted line on the left hand panel) are not used in the GA-LEI because the early-time data are contaminated by imperfect bucking of the primary field due to parasitic capacitance effects (Macnae and Baron-Hay, 2010). The parasitic capacitance typically leads to transients that rise at early-time, rather than decay as would be the case if the response was pure secondary field. All windows are used in the EM Flow™ CDI algorithm because it specifically attempts to account for the parasitic capacitance effects.

Firstly, note that the filtered (blue) and drift corrected (green) data are mostly obscured by the final levelled data. This is because the drift and levelling corrections in this case are small compared to the amplitude of the data. The main correction is at early time (<0.1 ms delay time) where the drift correction is typically large. However over the remainder of the transient the corrections are small and the transients plot coincident with each other. This indicates that the signal-to-data correction ratio, and hence the signal-to-noise ratio is large in this conductive area.

Secondly, it can also be seen in Figure 13 that the GA-LEI model (magenta) has been able to fit the final levelled (black) data transient within the estimated error, except at very early time where the data are not used in the inversion. Note also in the left hand

panel of Figure 13 that the forward model of the EM Flow™ CDI (red) does not match the final levelled data – its values are of the order of a factor 2 to 3 times smaller than the input data. Although we might have expected the match to be better, the EM Flow™ CDI algorithm is a fast approximate transformation rather than a data fitting inversion. Notwithstanding this, as noted earlier in the discussion on Figure 12, the GA-LEI and CDI conductivity sections are qualitatively similar.

4.2 Resistive areas of the Kombolgie dataset

We turn our attention now to an example of a more resistive part of the survey area, Line 20390, whose GA-LEI and EM Flow™ CDI conductivity sections are shown in Figure 14. The two sections are quite different in this case. The GA-LEI has resolved a broad smooth (weak) conductor over the top ~250 m depth, below which it is largely lacking coherent character. On the other hand the EM Flow™ CDI shows a thin conductor at the surface and a more prominent thin conductor at ~250 m depth (i.e., approximately at the base of the smooth GA-LEI conductor). The CDI also contains the deeper (~1000 m) and thicker (~750 m) conductor that is not apparent in the GA-LEI.

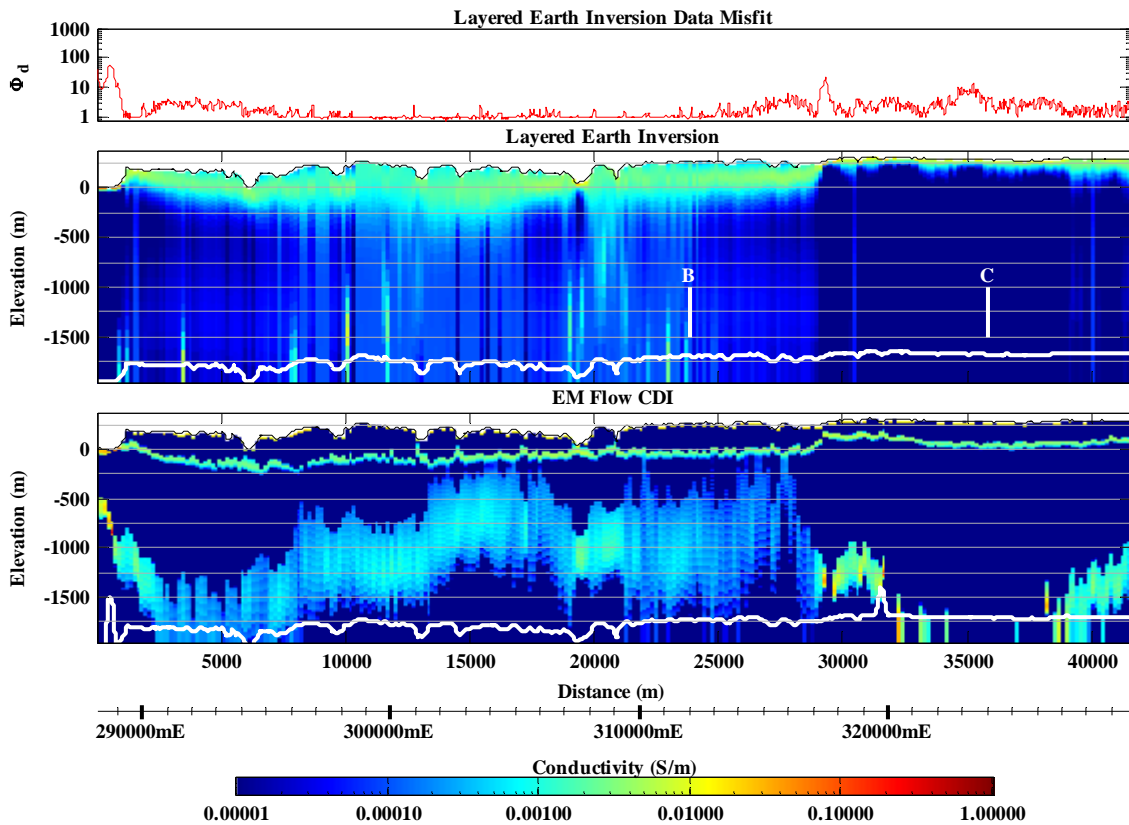


Figure 14: GA-LEI and EM Flow™ conductivity sections from a resistive part (Line 20390) of the Kombolgie survey area.

The details of the data and fitted models at positions ‘B’ and ‘C’ marked on the conductivity sections in Figure 14 are shown in Figure 15 and Figure 17 respectively. In the left hand panel of Figure 15 it can be seen that the drift correction that was applied to the data at ‘B’ (i.e., the difference between the green and blue transients) is

an order of magnitude larger than the final levelled data (black). This means that drift or zero-level error makes up the majority of the total measured response in this resistive area. With this in mind, it is clear that small relative errors in the drift correction estimated from high-altitude data will translate into significantly larger relative errors in the drift corrected and the final levelled data.

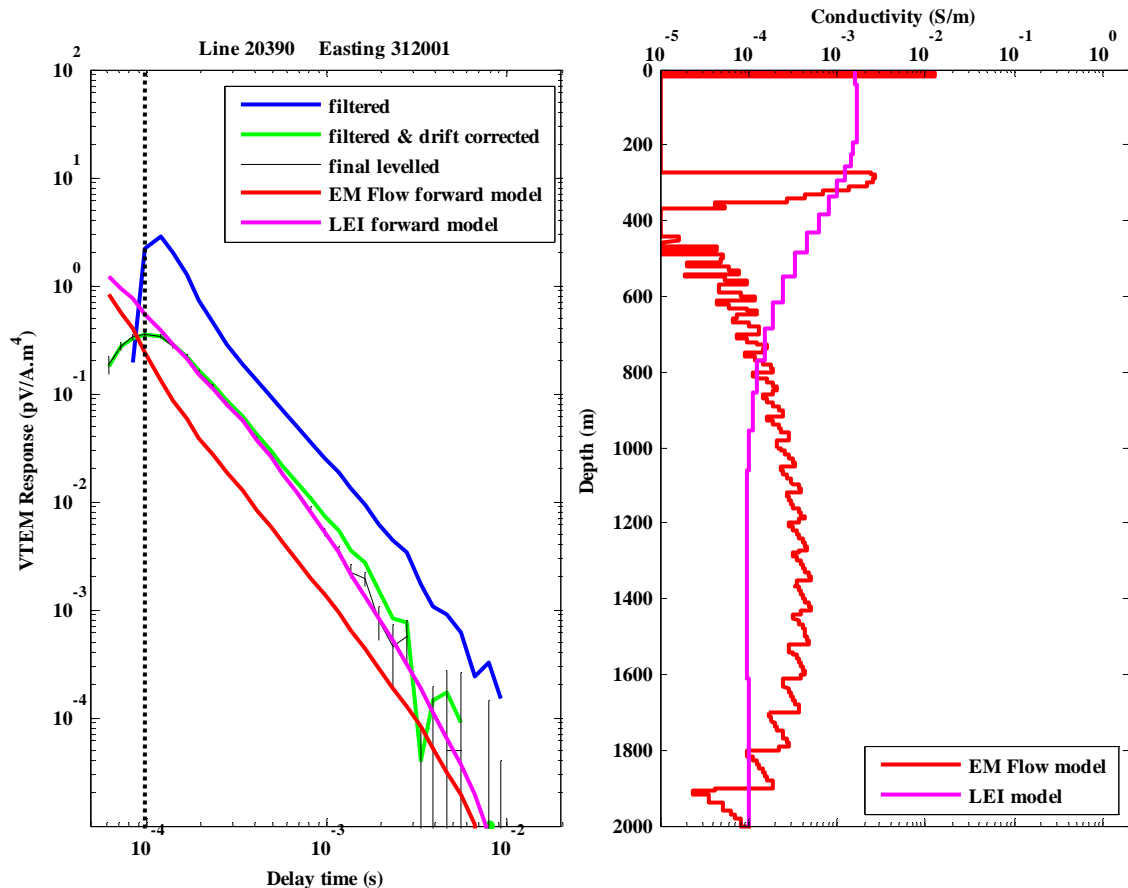


Figure 15: VTEM™ data (left) at the sample located at 'B' on Figure 14 and the corresponding GA-LEI and EM Flow™ CDI conductivity models (right).

4.3 Deep conductor in resistive areas

It can also be seen in Figure 15 that there is a good match between the final levelled data (black) and the forward model response of the GA-LEI inversion model (magenta). This is also reflected in the low data misfit (top panel) shown in Figure 14. Because the data were fitted satisfactorily by the GA-LEI, without the deep and thick conductor that is apparent in the corresponding EM Flow™ CDI section, we can say it was not required by the data. It is not clear to us what is causing the need for the deep conductor in the EM Flow™ CDI section. Thus Geoscience Australia advises caution when attempting to make geological interpretations of the conductivity sections.

However, on the other hand we are not suggesting that these deep conductors are simply artefacts. Geoscience Australia can also point to other flight lines where the GA-LEI

does require a deeper conductor, with similar character to that in the corresponding EM Flow™ CDI section, to adequately fit the data. One such example is shown in Figure 16.

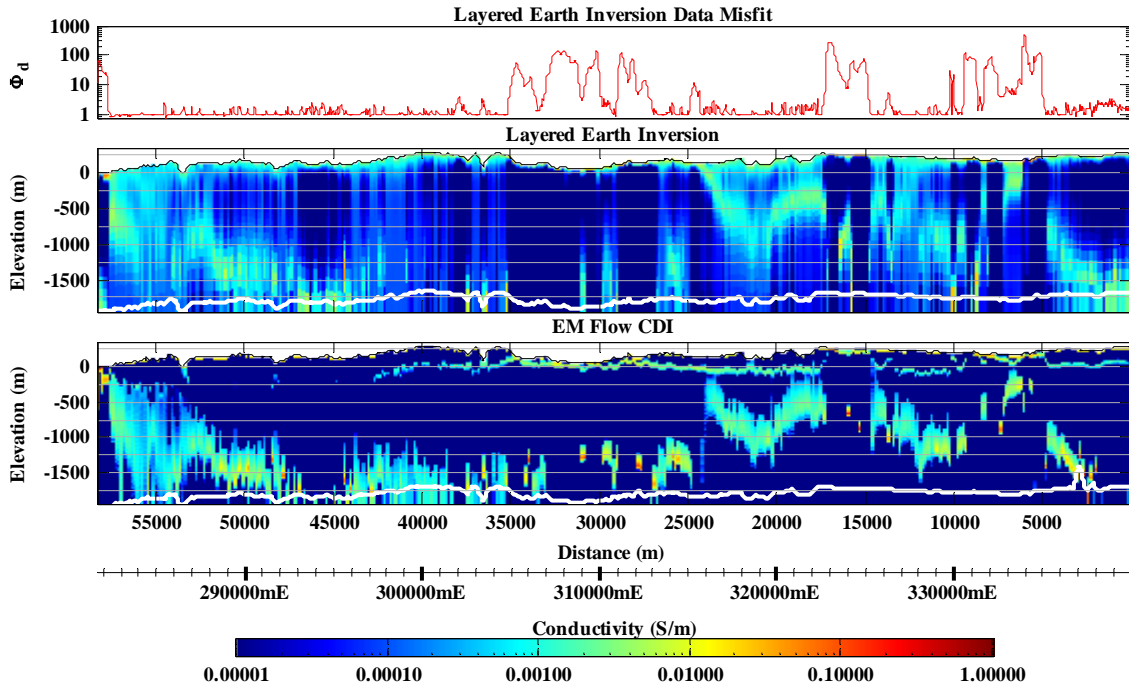


Figure 16: GA-LEI and EM Flow™ conductivity sections from a resistive part (Line 12100) of the Kombolgie survey area.

Figure 17 shows the details of the data and models at location ‘C’ marked on Figure 14, which is 12 kilometres further along the same flight line. Here the deeper conductor is absent from both the GA-LEI and the EM Flow™ CDI sections. Here the final levelled data (black) transient decays rapidly from ~ 0.0004 s, after which neither the GA-LEI nor the EM Flow™ CDI can fit the data. Here a large levelling correction (i.e., the difference between the black and green transients) has been applied to the late-time data in the last step of data processing. The justification for this correction is not clear, however it has had the effect of pushing the deeper conductor off the bottom of the EM Flow™ CDI section between easting 321000 mE and 326000 mE (bottom panel of Figure 14).

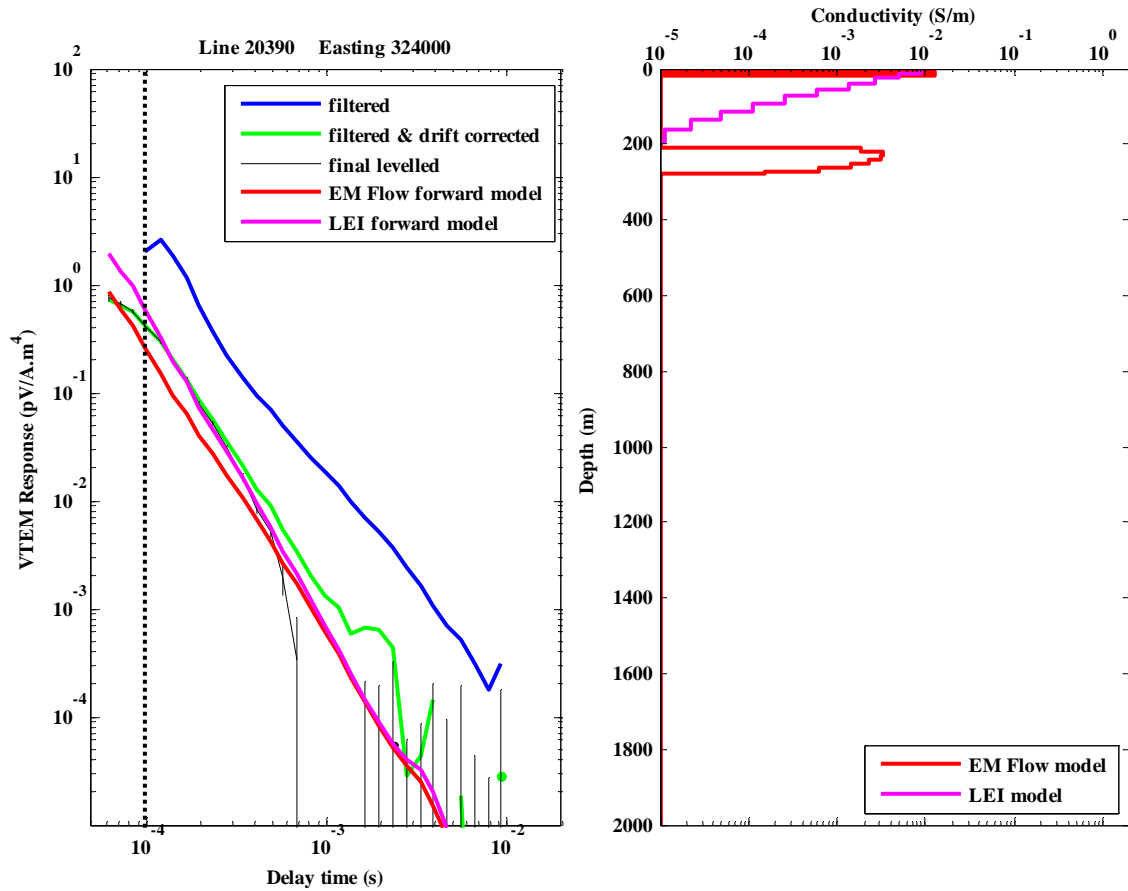


Figure 17: VTEM™ data (left) at the sample located at 'C' on Figure 14 and the corresponding GA-LEI and EM Flow™ CDI conductivity models (right).

Figure 18 shows the same conductivity sections as in Figure 14 (i.e., Line 20390), except in this case the GA-LEI and EM Flow™ CDI conductivity sections were generated from the drift corrected data (green transients on Figure 1.4 and Figure 1.5) instead of the final levelled data (black transients on Figure 1.4 and Figure 1.5). By comparing Figure 14 with Figure 18 in the portion of the line east of 317000 mE, it is clear that the final manually-derived levelling correction has 'broken-up' the more continuous deep conductor that would have been derived from the data prior to final levelling. This highlights the impact that subjective manually determined levelling corrections can have on the dataset, and gives reason to Geoscience Australia's advice of caution when attempting to make geological interpretations of the conductivity sections.

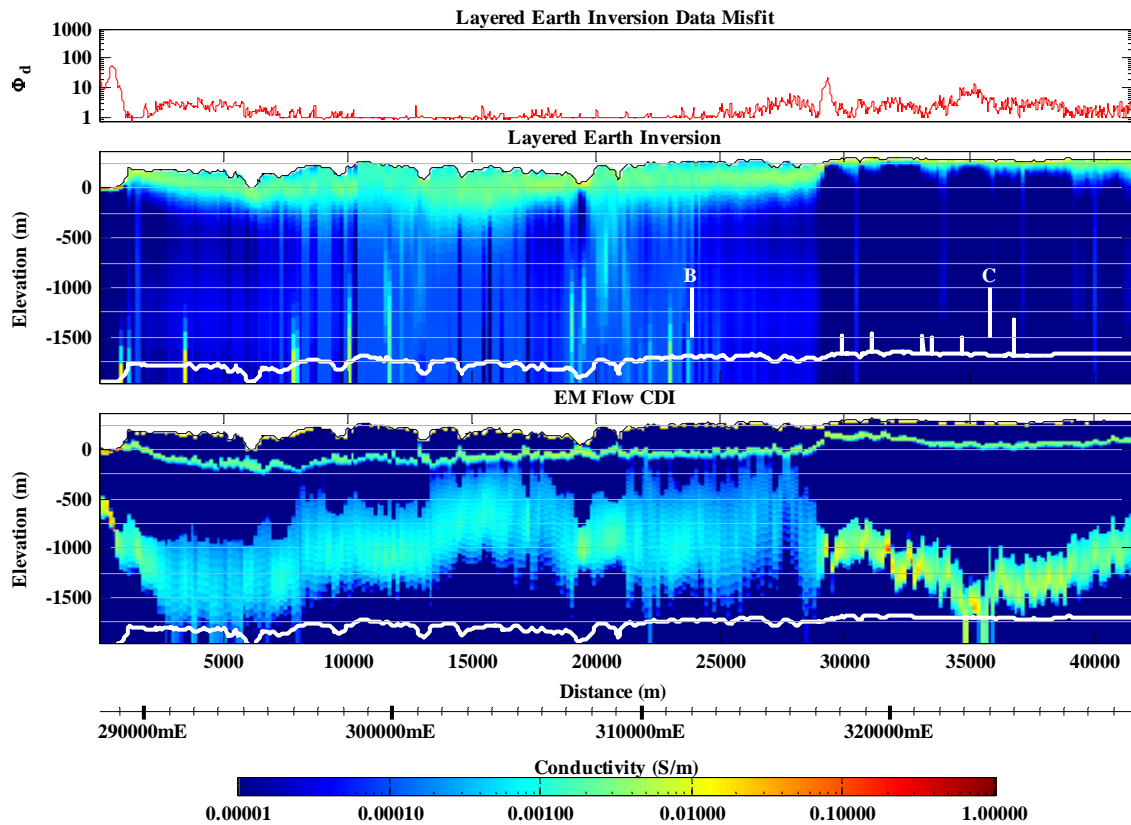


Figure 18: Similar to Figure 14, except in this case conductivity sections were generated from the drift corrected data (i.e., green transients on Figure 15) instead of the final levelled data (black transients).

4.4 Shallow conductor in resistive areas

We now turn our attention back to the shallow (<250 m) portion of the conductivity sections for Line 20390 (Figure 14 and Figure 18). Here the GA-LEI resolved a smooth broad conductor and the EM Flow™ CDI resolved a thin conductor at the surface and a more prominent thin conductor at ~250 m depth (i.e., approximately at the base of the smooth GA-LEI conductor).

The information shown in Figure 19 demonstrates the degree of ambiguity in the resolved models in the shallow zone. In similar fashion to Figure 15, it shows the details of the data and the GA-LEI and EM Flow™ CDI models at location 'B' marked on Figure 14 and Figure 18. However, it also includes two additional models, denoted alternate-1 and alternate-2, that fit the data just as well as the GA-LEI. Again it can be seen that a layered-earth forward model of the EM Flow™ CDI (red transient) does not match the final levelled data (black transient). However, the model alternate-2 (blue) does fit the data reasonably well.

This suggests that a thin-layer model, similar in geological character to that shown on the upper ~250 m of the EM Flow™ CDI conductivity sections, is plausible. However, in this case, the layered-earth modelling suggests that it is likely to be somewhat

(~130 m) shallower. Notwithstanding this, the broader and smoother GA-LEI and the alternate-1 models are also just as likely.

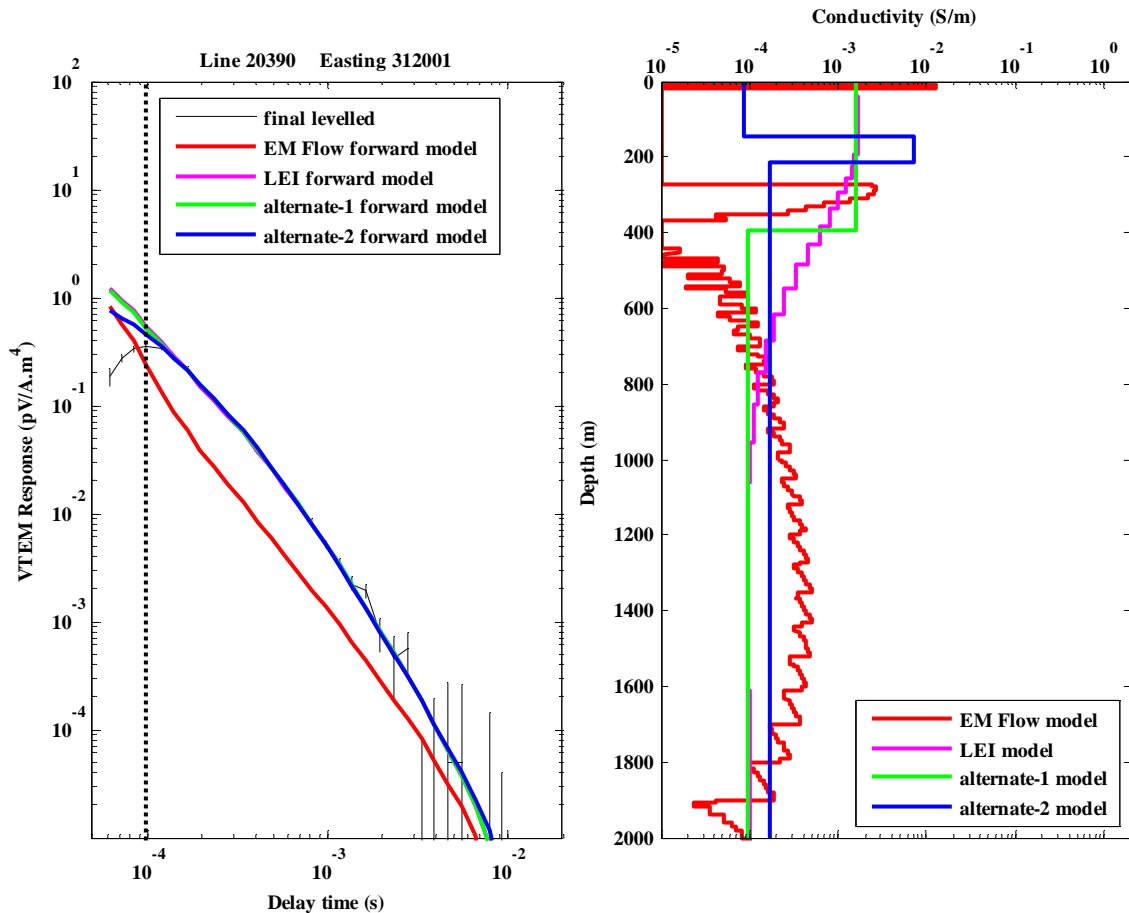


Figure 19: VTEM™ data (left) at the sample located at 'B' on Figure 14 and the corresponding GA-LEI and EM Flow™ CDI conductivity models, and two alternative models that also fit the data (right).

Geoscience Australia has access to a confidential industry log through the Kombolgie Subgroup into the basement below the unconformity. This single resistivity log shows the unconformity is more conductive than the rocks above and below it. This therefore supports the thin shallow conductor model (EM Flow™ CDI and Alternate-2) rather than the broader smoother model (GA-LEI and Alternate-1).

Acknowledgements

We acknowledge the significant contributions of Richard Lane to the Kombolgie AEM survey results. We would like to thank Professor James Macnae (RMIT) who greatly assisted GA through technical advice, provision of the most recent EM Flow™ research version software and help to determine the most appropriate waveform and program settings.

Geoscience Australia would also like to acknowledge the contributions of the following groups:

Northern Territory Geological Survey (NTGS); National Water Commission Natural Resources, Environment, The Arts and Sport (NRETAS), in particular Jon Sumner; Cameco Australia, in particular Geoff Beckitt and Tyler Mathieson; and Energy Resources of Australia Ltd. for field support as well as land access, access to open bore hole and lithological logs supporting the conductivity logging phase of the program. Subscription companies United Uranium Ltd., and Uranex NL for their support of the AEM project by funding additional lines, supplying historical data and providing geological support. The Northern Land Council, for granting access to traditional lands. We also thank the Geophysics Group and the Groundwater Group at GA, in particular Camilla Sorensen and Pauline English.

References

- Brodie, R., 2009a. Kombolgie VTEM Survey: GA Comments on Revised Bathymetry Calibration Line Data. Unpublished Geoscience Australia internal report.
- Brodie, R., 2009b. Kombolgie VTEM Survey: Note on loop position estimates. Unpublished Geoscience Australia internal report.
- Brodie, R. and Fisher, A., 2008. Inversion of TEMPEST AEM survey data, Honeysuckle Creek, Victoria. Unpublished report produced by Geoscience Australia for the Bureau of Rural Sciences.
- Carter S., Baron-Hay., Combrinck M. and Moreton M. 2009. Survey and Logistics report on a helicopter borne versatile time domain electromagnetic (VTEM) survey for the Pine Creek (Kombolgie) Project area Northern Territory.
https://www.ga.gov.au/products/servlet/controller?event=GEOCAT_DETAILS&catno=69230
- Christiansen, A. and Auken, E. 2010. A global measure for depth of investigation in EM and DC modeling. *ASEG Extended Abstracts*, 2010.
- Constable, S., Parker, R., and Constable, C., 1987. Occam's inversion; a practical algorithm for generating smooth models from electromagnetic sounding data. *Geophysics*, **52**, 289-300.
- Costelloe, M. and Brodie, R.C., 2011. Kombolgie AEM survey images to 2 km. *Preview*, **150**, 29-32.
- Costelloe, M., Sorensen, C. and English, P., 2009. Pine Creek Airborne Electromagnetic Survey Onshore Energy and Minerals, Geoscience Australia. *ASEG Extended Abstracts* 2009.
- Craig, M.A. ed. 2011. Geological and energy implications of the Pine Creek region airborne electromagnetic (AEM) survey, Northern Territory, Australia. Geoscience Australia **Record 2011/18**.
- Geotech, 2009a. Photo evidence of loop geometry. Unpublished report produced by Geotech for Geoscience Australia.
- Geotech, 2009b. Geotech Airborne Pty Ltd VTEM Transmitter Loop GPS and Altimeter Tests Flown 1st – 2nd April 2009. Unpublished report produced by Geotech for Geoscience Australia.
- Green, A. and Lane, R., 2003. Estimating noise levels in AEM data. *ASEG Extended Abstracts* 2003.

Lane, R., Brodie, R. and Fitzpatrick, A., 2004. Constrained inversion of AEM data from the Lower Balonne area, Southern Queensland, Australia. CRC LEME Open File Report 163.

Macnae, J. and Baron-Hay, S., 2010. Reprocessing strategy to obtain quantitative early time data from historic VTEM surveys: *ASEG Extended Abstracts* 2010.

Macnae, J., King, A., Stolz, N., Osmakoff, A., Blaha, A., 1998. Fast AEM processing and inversion: *Exploration Geophysics* **29**, 163-169.

Reid, J.E., and Brodie, R.C., 2006. Preliminary inversions of Honeysuckle Creek airborne electromagnetic data: Comparison with borehole conductivity logs and previously derived conductivity models. Unpublished report produced by Geoscience Australia for the Bureau of Rural Sciences.

Stolz, E., and Macnae, J., 1998. Evaluating EM waveforms by singular-value decomposition of exponential basis functions: *Geophysics*, **63**, 64-74.

Smith, R.S., 2001 On removing the primary field from fixed wing time-domain airborne electromagnetic data: some consequences for quantitative modelling, estimating bird position and detecting perfect conductors. *Geophysical Prospecting*, 49, 405-416.

Smith, R., and Annan, P., 2000. Using an induction coil sensor to indirectly measure the B-field response in the bandwidth of the transient electromagnetic method: *Geophysics*, **65**, 1489-1494.

Appendix A GA-LEI inversion algorithm

A.1 Introduction

The GA-LEI inversion program is capable of inverting data from most airborne time-domain AEM systems. It has the capability of inverting for layer conductivities, layer thicknesses, and system geometry parameters, or some subset of these. There are options to use a multi-layer smooth-model formulation (Constable *et al.*, 1987) or a few-layer blocky-model formulation (Sattel, 1998). For the sake of simplicity, only the aspects of the algorithm that are relevant to the inversion of TEMPEST data using a multi-layer smooth-model are described here.

TEMPEST data consist of a collection (tens of thousands to millions) of point located multi-channel samples acquired at 0.2 s (approximately 12 m) intervals along survey flight lines. The algorithm independently inverts each sample. The data inputs to the inversion of each sample are the observed total (primary plus secondary) field X-component and Z-component data. Auxiliary information input into the algorithm are the measured and assumed elements of the system geometry, the thicknesses of the layers, and prior information on the unmeasured elements of the system geometry and ground conductivity. The unknowns solved for in the inversion (outputs) are the electrical conductivity of the layers and the unmeasured elements of the system geometry.

Since each sample is inverted independently, the user may elect to invert all samples or some subset of them. The inversion of each sample results in an estimate of a one dimensional (1D) conductivity structure associated with that sample. Each estimated 1D conductivity structure, although theoretically laterally constant and extending infinitely in all directions, is only supported by the data within the system footprint which is approximately a square of side length 470 m centred about the sample point (Reid and Vrbancich, 2004). So by progressively inverting all the samples and stitching together the resultant 1D conductivity structures a depiction of the overall laterally variable 3D conductivity structure is built up.

A.2 Formulation

Figure A.20 shows the overall framework under which the inversion of a single airborne sample is carried out. The elements of the figure are progressively described in the following sections.

A.3 Coordinate System

Since each sample is inverted separately the coordinate system is different for the inversion of each sample. A right handed xyz Cartesian coordinate system is used. The origin of the coordinate system is on the Earth's surface directly below the centre of the transmitter loop. The x-axis is in the direction of flight of the aircraft at that sample

location, the y-axis is in the direction of the left wing and the z-axis is directed vertically upwards.

A.4 System Geometry

The centre of the transmitter loop is located at $(0, 0, TX_h)$. Roll of the transmitter loop (TX_r) is defined as anti-clockwise rotation, about an axis through $(0, 0, TX_h)$ and parallel to the x-axis, so that a positive roll will bring the left wing up. Pitch of the transmitter loop (TX_p) is defined as anti-clockwise rotation, about an axis through $(0, 0, TX_h)$ and parallel to the y-axis, so that positive pitch will bring the aircraft's nose down. Yaw of the transmitter loop (TX_y) is defined as anti-clockwise rotation, about an axis through $(0, 0, TX_h)$ and parallel to the z-axis, so that a positive yaw would turn the aircraft left. However since the x-axis is defined to be in the direction of flight at each sample, the transmitter loop yaw is always zero by definition. The order of operations for calculating the vector orientations is to apply the pitch, roll then yaw rotations respectively.

The position of the receiver coils relative to the transmitter loop is defined by the transmitter to receiver horizontal inline separation (D_x), the transmitter to receiver horizontal transverse separation (D_y), and the transmitter to receiver vertical separation (D_z). The receiver coils are thus located at $(D_x, D_y, RX_h=TX_h+D_z)$. The receiver coils are always behind and below the aircraft ($D_x < 0, D_z < 0$). The receiver coils' roll (RX_r), pitch (RX_p) and yaw (RX_y) have the same rotational convention as for the transmitter loop except that they are rotations about the point (D_x, D_y, D_z) . The receiver coils are always assumed to be located on the y-axis ($D_y = 0$) and to have zero yaw ($RX_y = 0$). Although this is not in reality the case, the position and orientation is not measured and there is not enough information available to solve for these since Y-component data is not available.

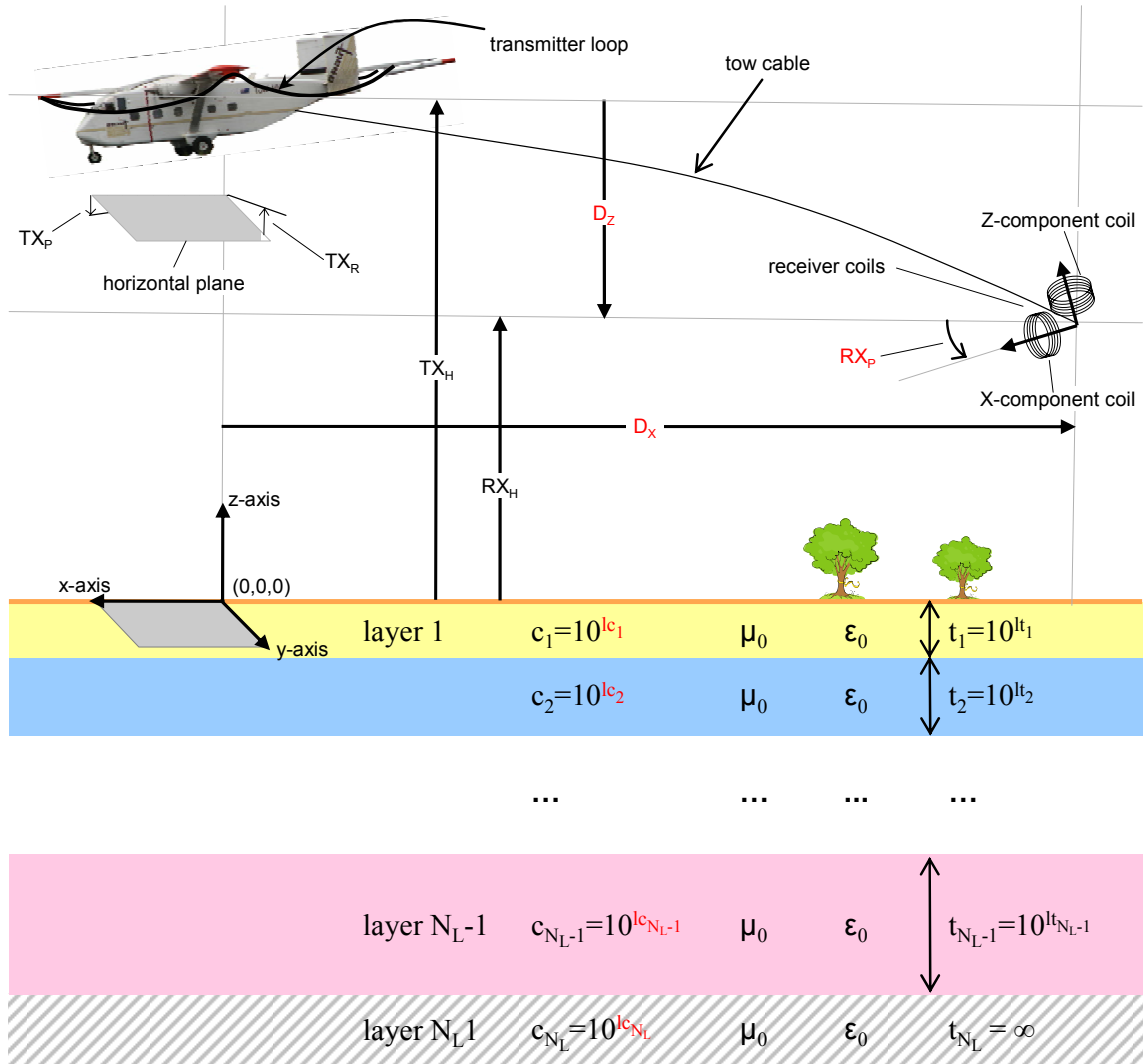


Figure A.20: Schematic representation of the framework for GA-LEI inversion of TEMPEST AEM data. Red elements are the unknowns to be solved for.

Note that transmitter loop pitch data supplied by Fugro Airborne Surveys in processed TEMPEST data uses the convention where a positive transmitter pitch is nose up, and accordingly the supplied pitch is reversed in sign before being used in the inversion algorithm.

A.5 Layered Earth

The layered earth model is independent at each inverted sample location. The layered earth consists of N_L horizontal layers stacked on top of each other in layer cake fashion. The k^{th} layer has constant thickness t_k and the bottom layer is a halfspace that has infinite thickness ($t_{N_L} = \infty$), extending to infinite depth. The electrical conductivity of the k^{th} layer is c_k and it is constant throughout the layer. The magnetic permeability of all layers is assumed to be equal to the magnetic permeability of free space μ_0 . The dielectric permittivity of all layers is assumed to be equal to the permittivity of free space ϵ_0 .

A.6 Data

Part of the TEMPEST data processing sequence involves partitioning the total (secondary plus primary) field response that is actually observed into estimates of the unknown primary and secondary field components. Then an estimate of the transmitter to receiver horizontal in-line and vertical separations D_x and D_z are made from the partitioned primary field component. The procedure uses the measured transmitter pitch (TX_p) and roll (TX_r) and assumes the receiver coils are flying straight, level and directly behind the aircraft ($D_y=0$, $RX_r=0$, $RX_p=0$, and $RX_y=0$). It is the estimated secondary field data, the measured elements of the system geometry (TX_h , TX_p , TX_r , and TX_y) and the associated estimates of the unmeasured elements of the system geometry (D_x and D_z) that are delivered to clients. Implicit in the delivered dataset are the assumed elements of the system geometry ($D_y=0$, $RX_r=0$, $RX_p=0$, and $RX_y=0$). However the estimated primary field data are not delivered to clients.

Since the GA-LEI algorithm makes its own estimate of system geometry as part of the inversion procedure it works with total field data. The input data are the total (primary plus secondary) field X-component and Z-component data. Therefore the total field data are first reconstructed. This is a simple matter of recomputing the primary field from magnetic dipole formulae (Wait, 1982) using the delivered (measured, estimated and assumed) elements of the system geometry then adding them to the delivered secondary field data. Note that the height, pitch, roll and geometry corrected data that are usually delivered as part of TEMPEST datasets are not used because the GA-LEI algorithm makes its own estimate of system geometry as part of the inversion procedure.

The reconstructed X-component and Z-component total field data for the k^{th} window are $X_k = X^P + X_k^S$ and $Z_k = Z^P + Z_k^S$ respectively. Here the super scripts P and S represent primary and secondary field components. Since the TEMPEST system has $N_w = 15$ windows, the observed data vector of length $N_D = 2 \times N_w = 30$ used in the inversion is,

$$\mathbf{d}^{obs} = [X_1 \ X_2 \ \dots X_{N_w} \ Z_1 \ Z_2 \ \dots Z_{N_w}]^T \quad (1)$$

where T represents the matrix and vector transpose operator.

Errors on the data are calculated outside of the program and input along with the data. Errors are assumed to be uncorrelated and Gaussian distributed. They are estimated as standard deviations of the Gaussian error distribution for each window and receiver component. Typically errors are calculated from the parameters of an additive plus multiplicative noise model (Green and Lane, 2003). Parameters of the noise model are determined from analysis of high altitude and repeat line data. If X_k^{err} and Z_k^{err} , represent the estimated standard deviation of the error in the k^{th} window of the X-component and Z-component data respectively then the data error vector of length $N_D=30$ is,

$$\mathbf{d}^{err} = [X_1^{err} \ X_2^{err} \ \dots X_{N_w}^{err} \ Z_1^{err} \ Z_2^{err} \ \dots Z_{N_w}^{err}]^T. \quad (2)$$

A.7 Model Parameterisation

The unknown model parameter vector (**m**) to be solved for in the inversion comprises earth model parameters and system geometry model parameters.

For the inversion of the TEMPEST dataset described here we choose to use a multi-layer smooth-model formulation (Constable *et al.*, 1987) rather than a few-layer blocky-model formulation (Sattel, 1998). Therefore we solve for the N_L conductivities of the layers but not the thicknesses. The layer thicknesses are inputs into the algorithm and are kept fixed throughout. To maintain positivity of the layer conductivities we actually invert for the base ten logarithms of the conductivities of each layer.

We solve for $N_G=3$ system geometry parameters: the transmitter to receiver horizontal in-line separation (D_x), the transmitter to receiver vertical separation (D_z), and the pitch of the receiver coil assembly (RX_p).

The unknown model parameter vector of length $N_p=N_G + N_L$ to be solved for is the concatenated vector of log base ten layer conductivities $\mathbf{lc} = [\log c_1 \log c_2 \cdots \log c_{N_L}]^T$ and the geometry parameters $\mathbf{g} = [D_x \ D_z \ RX_p]^T$, such that,

$$\mathbf{m} = [\mathbf{lc} \mid \mathbf{g}] = [\log c_1 \log c_2 \cdots \log c_{N_L} \ D_x \ D_z \ RX_p]^T \quad (3)$$

A.8 Forward Model Derivatives

The forward model is the non-linear multi-valued function,

$$\mathbf{f}(\mathbf{m}) = [f_1(\mathbf{m}, \mathbf{p}) \ f_2(\mathbf{m}, \mathbf{p}) \cdots f_{ND}(\mathbf{m}, \mathbf{p})], \quad (4)$$

which for a given a set of model parameters (**m**) calculates the theoretical total field data equivalent to that which would be produced for an ideal system, after the measurement and transformation by the data processing steps (Lane *et al.*, 2000). Here each $f_k(\mathbf{m}, \mathbf{p})$ is a function, not only of the layer conductivities and system geometry parameters in the inversion model vector **m**, but also of several other fixed parameters **p** (layer thicknesses; transmitter height, pitch and roll; receiver roll and yaw, transmitter to receiver horizontal transverse separation; system waveform and window positions *etc.*).

The implementation of (4) is based upon the formulation of Wait (1982) in which he develops the frequency-domain expressions for the magnetic fields due to vertical and horizontal magnetic dipole sources above a horizontally layered medium. The formulation does not account for the contribution due to displacement currents. We also assume that effects of dielectric permittivity and magnetic susceptibility are negligible compared to electrical conduction, and set each layer's dielectric permittivity and magnetic permeability to that of free space ($\epsilon_k=\epsilon_0$; $\mu_k=\mu_0$).

The full transient (0.04 s) equivalent square current waveform, to which TEMPEST data are processed, was linearly sampled at 75,000 Hz (3000 samples) and transformed to the frequency domain via fast Fourier transform (FFT). Using Wait's expressions the secondary B-field was calculated for ~20 discrete frequencies between 25 Hz and 37,500 Hz (6 logarithmically equi-spaced frequencies per decade). The inphase and quadrature parts of each component were then individually splined to obtain linearly spaced values at the same frequencies as the nodes of the FFT transformed current

waveform. Complex multiplication of splined B-field with the FFT transformed current waveform, followed by inverse FFT, yielded the B field transient response.

The transient was then windowed (boxcar) into the 15 windows by averaging those samples that fell within each window. The primary field, which is constant over all 15 windows, was then computed from Wait's expressions and added to yield the total field window response in the x -axis and z -axis directions. Finally these were rotated to be aligned with the X-component receiver coil's axis and Z-component receiver coil's axis according to the receiver pitch model parameter (RX_p) to yield $\mathbf{f}(\mathbf{m})$.

The inversion also requires the partial derivatives of $\mathbf{f}(\mathbf{m})$ with respect to the model parameters (see Equation 19). These were all calculated analytically. For computation of Wait's coefficient R_0 , we took advantage of the propagation matrix method (Farquharson *et al.*, 2004) because it is efficient for computation of the partial derivatives with respect to the multiple layer conductivities.

A.9 Reference Model

The algorithm uses the concept of a reference model (Farquharson and Oldenburg, 1993) to incorporate prior information from downhole conductivity logs or lithologic/stratigraphic logging in order to improve inversion stability and to reduce the trade-off between parameters that are not well resolved independently. Since prior information is not available everywhere within the survey area, and the inversions are carried out in independent sample by sample fashion, it is not plausible to place hard reference model constraints on the model parameters. Instead the reference model provides a soft or probabilistic constraint only. If, from prior information, it is concluded that the likely distribution of the model parameter m_k is a Gaussian distribution with mean m_k^{ref} and standard deviation m_k^{unc} , then we would define the reference model vector as,

$$\mathbf{m}^{ref} = [lc_1^{ref} \quad lc_2^{ref} \quad \dots \quad lc_{N_L}^{ref} \quad D_x^{ref} \quad D_z^{ref} \quad RX_p^{ref}]^T \quad (5)$$

and the reference model uncertainty vector as,

$$\mathbf{m}^{unc} = [lc_1^{unc} \quad lc_2^{unc} \quad \dots \quad lc_{N_L}^{unc} \quad D_x^{unc} \quad D_z^{unc} \quad RX_p^{unc}]^T \quad (6)$$

The reference model mean values and uncertainties are inputs to the inversion algorithm and they may be different from sample to sample. The uncertainty values assigned to the reference model control the amount of constraint that the reference model places on the inversion results. A large uncertainty value for a particular parameter implies that the assigned reference model mean value is not well known and thus is allowed to vary a long way from the mean. On the other hand a low uncertainty implies the parameter is well known.

A.10 Objective Function

The inversion scheme minimises a composite objective function of the form,

$$\Phi = \Phi_d + \lambda (\alpha_c \Phi_c + \alpha_g \Phi_g + \alpha_v \Phi_v) \quad (7)$$

where Φ_d is a data misfit term, Φ_c is a layer conductivity reference model misfit term, Φ_g is a system geometry reference model misfit term, and Φ_v is a vertical roughness of conductivity term. The relative weighting of the data misfit Φ_d and the collective model regularisation term,

$$\Phi_m = \alpha_c \Phi_c + \alpha_g \Phi_g + \alpha_v \Phi_v \quad (8)$$

is controlled by the value of regularisation factor λ . The three model regularisation factors α_c , α_g and α_v control the relative weighting within the model regularisation term Φ_m . The algorithm requires that the α values be set by the user on a application by application basis and they remain fixed throughout the inversion. However the λ is automatically determined within the algorithm by the method described in Section A.17.

A.11 Data Misfit

The data misfit Φ_d is a measure of the misfit, between the data (\mathbf{d}^{obs}) and the forward model of the model parameters ($\mathbf{f}(\mathbf{m})$), normalised by the expected error and the number of data. It is defined as,

$$\Phi_d = \frac{1}{N_D} \sum_{k=1}^{N_D} \left(\frac{d_k^{obs} - \mathbf{f}(\mathbf{m})}{d_k^{err}} \right)^2 \quad (9)$$

$$= \left[\mathbf{d}^{obs} - \frac{\mathbf{f}(\mathbf{m})}{(d_1^{err})} \right]^T \mathbf{W}_d \left[\mathbf{d}^{obs} - \mathbf{f}(\mathbf{m}) \right]$$

The diagonal $N_D \times N_D$ matrix \mathbf{W}_d is,

$$\mathbf{W}_d = \frac{1}{N_D} \frac{1}{(d_2^{err})^2} \quad (10)$$

A.12 Conductivity Reference Model Misfit

The conductivity reference model misfit term Φ_c is a measure of the misfit, between the logarithmic conductivity model parameters ($\mathbf{l}\mathbf{c}$) and the corresponding layer reference model values ($\mathbf{l}\mathbf{c}^{ref}$) normalised by the layer thicknesses and reference model uncertainty. It is defined as,

$$\Phi_c = \sum_{k=1}^{N_L} \frac{t_k}{T/N_L} \left(\frac{lc_k^{ref} - lc_k}{lc_k^{unc}} \right)^2 \quad (11)$$

$$= \left[\mathbf{m}^{ref} - \mathbf{m} \right]^T \mathbf{W}_c \left[\mathbf{m}^{ref} - \mathbf{m} \right]$$

where $T = \sum_{k=1}^{N_L} t_k$, and the diagonal $N_p \times N_p$ matrix \mathbf{W}_c is,

$$\mathbf{W}_c = \frac{N_L}{T} \begin{bmatrix} \frac{t_1}{(lc_1^{unc})^2} & & & & & \\ & \frac{t_2}{(lc_2^{unc})^2} & & & & \\ & & \dots & & & \\ & & & \frac{t_{N_L-1}}{(lc_{N_L-1}^{unc})^2} & & \\ & & & & \frac{t_{N_L}}{(lc_{N_L}^{unc})^2} & \\ & & & & & 0 \\ & & & & & & 0 \\ & & & & & & & 0 \end{bmatrix}. \quad (12)$$

Since the bottom layer is infinitely thick, for the purposes of this term we set $t_{N_L} = [t_{N_L-1}]^2 / t_{N_L-2}$.

A.13 System Geometry Reference Model Misfit

The system geometry reference model misfit term Φ_g is a measure of the misfit, between the system geometry model parameters (\mathbf{g}) and the corresponding system geometry reference model values (\mathbf{g}^{ref}) normalised by the number of unknown system geometry parameters ($N_G=3$) and their uncertainty. It is defined as,

$$\begin{aligned} \Phi_g &= \frac{1}{N_G} \sum_{k=1}^{N_G} \left(\frac{\mathbf{g}_k^{ref} - \mathbf{g}_k}{\mathbf{g}_k^{unc}} \right)^2 \\ &= [\mathbf{m}^{ref} - \mathbf{m}]^T \mathbf{W}_g [\mathbf{m}^{ref} - \mathbf{m}] \end{aligned} \quad (13)$$

The diagonal $N_p \times N_p$ matrix \mathbf{W}_g is,

$$\mathbf{W}_g = \frac{1}{N_G} \begin{bmatrix} 0 & & & & & \\ & 0 & & & & \\ & & \dots & & & \\ & & & 0 & & \\ & & & & 0 & \\ & & & & & \frac{1}{(D_x^{unc})^2} \\ & & & & & & \frac{1}{(D_y^{unc})^2} \\ & & & & & & & \frac{1}{(RX_p^{unc})^2} \end{bmatrix}. \quad (14)$$

$$\Delta \mathbf{m}_n = \mathbf{m}_{n+1} - \mathbf{m}_n. \quad (18)$$

The forward model at the new set of model parameters \mathbf{m}_{n+1} is approximated by a Taylor series expansion about \mathbf{m}_n , which, after excluding high order terms reduces to,

$$\mathbf{f}(\mathbf{m}_{n+1}) \approx \mathbf{f}(\mathbf{m}_n) + \mathbf{J}_n(\mathbf{m}_{n+1} - \mathbf{m}_n) \quad (19)$$

where $\mathbf{J}_n = \partial \mathbf{f}(\mathbf{m}) / \partial \mathbf{m}$ is the Jacobian matrix whose i^{th} , j^{th} element is the partial derivative of the i^{th} datum with respect to the j^{th} model parameter evaluated at \mathbf{m}_n in model space. Making use of Equation 19 and substituting $\mathbf{m} = \mathbf{m}_{n+1}$, allows Equation 17 to be rewritten as,

$$\begin{aligned} \Phi(\mathbf{m}_{n+1}) = & \left[\mathbf{d}^{obs} - \mathbf{f}(\mathbf{m}_n) - \mathbf{J}_n(\mathbf{m}_{n+1} - \mathbf{m}_n) \right]^T \mathbf{W}_d \left[\mathbf{d}^{obs} - \mathbf{f}(\mathbf{m}_n) - \mathbf{J}_n(\mathbf{m}_{n+1} - \mathbf{m}_n) \right] \\ & + \lambda \alpha_c \left[\mathbf{m}^{ref} - \mathbf{m}_{n+1} \right]^T \mathbf{W}_c \left[\mathbf{m}^{ref} - \mathbf{m}_{n+1} \right] \\ & + \lambda \alpha_g \left[\mathbf{m}^{ref} - \mathbf{m}_{n+1} \right]^T \mathbf{W}_g \left[\mathbf{m}^{ref} - \mathbf{m}_{n+1} \right] \\ & + \lambda \alpha_v \mathbf{m}_{n+1}^T \mathbf{L}_v^T \mathbf{L}_v \mathbf{m}_{n+1} \end{aligned} \quad (20)$$

Since the value of Φ will be minimised when $\partial \Phi / \partial \mathbf{m}_{n+1} = 0$, we differentiate Equation 20 with respect to \mathbf{m}_{n+1} and set the result to zero and get,

$$\begin{aligned} 0 = & -2 \mathbf{J}_n^T \mathbf{W}_d \left[\mathbf{d}^{obs} - \mathbf{f}(\mathbf{m}_n) - \mathbf{J}_n(\mathbf{m}_{n+1} - \mathbf{m}_n) \right] \\ & + \lambda \left[-2 \alpha_c \mathbf{W}_c \left[\mathbf{m}^{ref} - \mathbf{m}_{n+1} \right] - 2 \alpha_g \mathbf{W}_g \left[\mathbf{m}^{ref} - \mathbf{m}_{n+1} \right] + 2 \alpha_v \mathbf{L}_v^T \mathbf{L}_v \mathbf{m}_{n+1} \right] \end{aligned} \quad (21)$$

Collecting terms in the unknown vector \mathbf{m}_{n+1} on the left hand side yields,

$$\begin{aligned} \left[\mathbf{J}_n^T \mathbf{W}_d \mathbf{J}_n + \lambda (\alpha_c \mathbf{W}_c + \alpha_g \mathbf{W}_g + \alpha_v \mathbf{L}_v^T \mathbf{L}_v) \right] \mathbf{m}_{n+1} = & \dots \\ \mathbf{J}_n^T \mathbf{W}_d \left[\mathbf{d}^{obs} - \mathbf{f}(\mathbf{m}_n) + \mathbf{J}_n \mathbf{m}_n \right] + \lambda [\alpha_c \mathbf{W}_c + \alpha_g \mathbf{W}_g] \mathbf{m}^{ref} \end{aligned} \quad (22)$$

Since Equation 22 is in the familiar form of a system of linear equations ($\mathbf{A} \mathbf{m}_{n+1} = \mathbf{b}$) we are able to solve for \mathbf{m}_{n+1} using a variety of linear algebra methods. We use Cholesky decomposition.

A.17 Choice of the value of λ

An initial value of λ is chosen such that the data and model objective functions will have approximately equal weight. This is automatically realised by computing the ratio of the data and model objective functions, from the reference model perturbed by 1%, and computing the ratio of the data and model misfits,

$$\lambda_{start} = \frac{\Phi_d(\mathbf{f}(1.01 \times \mathbf{m}_0))}{\Phi_m(1.01 \times \mathbf{m}_0)}. \quad (23)$$

Then at each iteration the inversion employs a 1D line search where, in solving for \mathbf{m}_{n+1} in Equation 22 different values of λ are trialled, until a value of λ_n is found such that,

$$\Phi_d(\mathbf{f}(\mathbf{m}_{n+1})) \approx \Phi_d^{target} = 0.7 \times \Phi_d(\mathbf{f}(\mathbf{m}_n)), \quad (24)$$

thus reducing Φ_d to 0.7 of its previous value.

A.18 Convergence Criterion

The iterations continue until the inversion terminates when one of the following conditions is encountered;

Φ_d reaches a user defined minimum value $\Phi_d^{\min} = 1$;

Φ_d has been reduced by less than 1% in two consecutive iterations;

Φ_d can no longer be reduced; or

the number of iterations reaches a maximum of 100 iterations.

A.19 References

Constable, S.C., Parker, R.L. and Constable, C.G., 1987. Occam's inversion: a practical inversion method for generating smooth models from electromagnetic sounding data. *Geophysics*, **52**, 289-300.

Farquharson, C.G., and Oldenburg, D.W., 1993. Inversion of time domain electromagnetic data for a horizontally layered earth. *Geophysical Journal International*, **114**, 433–442.

Farquharson, C. G., D. W. Oldenburg, and P. S. Routh, 2004, Simultaneous 1D inversion of loop-loop electromagnetic data for magnetic susceptibility and electrical conductivity. *Geophysics*, **68**, 1857–1869.

Green, A., and Lane, R., 2003. Estimating Noise Levels in AEM Data. Extended Abstract, ASEG 16th Geophysical Conference and Exhibition, February 2003, Adelaide.

Lane, R., Green, A., Golding, C., Owers, M., Pik, P., Plunkett, C., Sattel, D. and Thorn, B., 2000. An example of 3D conductivity mapping using the TEMPEST airborne electromagnetic system. *Exploration Geophysics*, **31**: 162-172.

Reid, J.E., and Vrbancich, J., 2004. A comparison of the inductive-limit footprints of airborne electromagnetic configurations. *Geophysics*, **69**, 1229–1239.

Sattel, D., 1998, Conductivity information in three dimensions. *Exploration Geophysics*, **29**, 157–162.

Wait, J.R., 1982, Geo-electromagnetism. Academic Press Inc.

Appendix B VTEM™ system file

```
System Begin
  Name = VTEM_Kombolgie
  Type = Time Domain
  Transmitter Begin
    NumberOfTurns = 1
    PeakCurrent = 1
    LoopArea = 1
    BaseFrequency = 25
    WaveFormCurrent Begin
      File = VTEM.cfm
    WaveFormCurrent End
    WaveformDigitisingFrequency = 409600
  Transmitter End
  Receiver Begin
    NumberOfWindows = 26
    WindowWeightingScheme = LinearTaper
    WindowTimes Begin
      0.0001093917      0.0001302083
      0.0001301917      0.0001510083
      0.0001510917      0.0001823083
      0.0001822917      0.0002135083
      0.0002135917      0.0002552083
      0.0002551917      0.0003073083
      0.0003072917      0.0003698083
      0.0003697917      0.0004427083
      0.0004426917      0.0005260083
      0.0005260917      0.0006198083
      0.0006197917      0.0007448083
      0.0007447917      0.0008906083
      0.0008905917      0.0010573083
      0.0010572917      0.0012448083
      0.0012447917      0.0014948083
      0.0014947917      0.0017865083
      0.0017864917      0.0021198083
      0.0021197917      0.0024948083
      0.0024947917      0.0029948083
      0.0029947917      0.0035781083
      0.0035780917      0.0042448083
      0.0042447917      0.0049948083
      0.0049947917      0.0059948083
      0.0059947917      0.0071615083
      0.0071614917      0.0084948083
      0.0084947917      0.0099948083
    WindowTimes End
  Receiver End

  ForwardModelling Begin
    OutputType = dB/dt
    XOutputScaling = 1e12
    YOutputScaling = 1e12
    ZOutputScaling = 1e12
    SecondaryFieldNormalisation = none
    FrequenciesPerDecade = 6
    NumberOfAbsiccaInHankelTransformEvaluation = 21
    SaveDiagnosticFiles = no
  ForwardModelling End
System End
```

Appendix C Inversion control file

```

Control Begin
  LogFile = inversion.output.log
  InfoFile = inversion_info.txt
  Matlab Begin
    Call = no
    PostIterationMFile = post_iteration.m
    PostSampleMFile = post_sample.m
    DumpPath = results\
  Matlab End
  EMSystem Begin
    SystemFile = /short/r17/aem/stmfiles/VTEM-26w.stm
    NumberOfWindows = 26
    UseXComponent = no
    UseYComponent = no
    UseZComponent = yes
    InvertTotalField = no
    ReconstructPrimaryFieldFromInputGeometry = no
    EstimateNoiseFromModel = yes
    ZMultiplicativeNoise = 3.6
    ZAdditiveNoise = 0.008194    0.005067    0.003395    0.002301
0.001758    0.001315    0.001035    0.000803    0.000689    0.000611    0.000504
0.000442    0.000391    0.000362    0.000323    0.000299    0.000277    0.000269
0.000245    0.000236    0.000225    0.000223    0.000215    0.000209    0.0002
0.000194
  EMSystem End
  Earth Begin
    NumberOfLayers = 30
  Earth End
  Options Begin
    SolveConductivity = yes
    SolveThickness = no
    SolveTX_Height = no
    SolveTX_Roll = no
    SolveTX_Pitch = no
    SolveTX_Yaw = no
    SolveTXRX_DX = no
    SolveTXRX_DY = no
    SolveTXRX_DZ = no
    SolveRX_Roll = no
    SolveRX_Pitch = no
    SolveRX_Yaw = no
    LambdaChoiceMethod = TargetLineSearchandStepFactor
    AlphaConductivity = 1.0
    AlphaThickness = 0.0
    AlphaGeometry = 0.0
    AlphaSmoothness = 1000000 //Set to 0 for no vertical conductivity
smoothing
    WeightConductivityReferenceByLayerThickness = yes
    WeightSmoothnessByLayerThickness = yes
    MinimumPhiD = 1.0
    MinimumPercentageImprovement = 0.1
    MaximumIterations = 100
  Options End
  InputOutput Begin
    InputFile =
/short/r17/aem/kombolgie/lines_survey_em_sub5/kombolgie_em_surveylines_sub5.dat
    HeaderLines = 0
    Subsample = 1
    OutputDataFile = inversion.output.asc
    OutputHeaderFile = inversion.output.hdr
    Columns Begin
      SurveyNumber = Column 1
      DateNumber = Column 6
    
```


Kombolgie VTEM™ AEM Survey: Inversion Report

```

FlightNumber      = Column 3
LineNumber        = Column 4
FidNumber         = Column 5
Easting           = Column 11
Northing          = Column 12
GroundElevation   = Column 19
Altimeter         = Column 17
TX_Height         = Column 26
TX_Roll           = 0
TX_Pitch          = 0
TX_Yaw            = 0
TXRX_DX           = 0
TXRX_DY           = 0
TXRX_DZ           = 0
RX_Roll           = 0
RX_Pitch          = 0
RX_Yaw            = 0
ReferenceModel Begin
    TX_Height      = Column 26
    Conductivity   = 0.0001
    Thickness      = 12.0 13.2 14.5 16.0 17.6 19.3 21.3 23.4 25.7 28.3
31.1 34.2 37.7 41.4 45.6 50.1 55.1 60.7 66.7 73.4 80.7 88.8 97.7 107.5 118.2 130.0 143.0
157.3 173.1
ReferenceModel End
StartModel Begin
    TX_Height      = Column 26
    Conductivity   = 0.0001
    Thickness      = 12.0 13.2 14.5 16.0 17.6 19.3 21.3 23.4 25.7 28.3
31.1 34.2 37.7 41.4 45.6 50.1 55.1 60.7 66.7 73.4 80.7 88.8 97.7 107.5 118.2 130.0 143.0
157.3 173.1
StartModel End
StdDevReferenceModel Begin
    TX_Height      = 10.0
    Conductivity   = 3.0
    Thickness      = 0.0
StdDevReferenceModel End
XComponentPrimary = UNAVAILABLE
YComponentPrimary = UNAVAILABLE
ZComponentPrimary = UNAVAILABLE
XComponentSecondary = UNAVAILABLE
YComponentSecondary = UNAVAILABLE
ZComponentSecondary = -Column 213
StdDevXComponentWindows = UNAVAILABLE
StdDevYComponentWindows = UNAVAILABLE
StdDevZComponentWindows = UNAVAILABLE
Columns End
InputOutput End
Control End

```

Appendix D Digital data package

The digital data package containing the inversion results and derived products is divided into several disk directories (folders). The contents of the package is described in the table below.

Directory\File	Format and description
.\ CC_license.pdf readme.txt kombolgie_LEI_report.pdf	package base (root) directory PDF file containing the data package licence ASCII text data package readme file PDF file containing this report
.\point_located\ kombolgie_lei.dat kombolgie_lei.dat.des kombolgie_lei.dat.dfn kombolgie_lei.dat.ddf	point located (line) inversion results flat ASCII columns data file ASEG-GDF2 descriptive header file ASEG-GDF2 column definition file Intrepid™ DDF import file <i>211 flight lines in one data file</i>
.\grids\layers\ conductivity_NN conductivity_NN.ers	layer conductivity grids ER Mapper™ grid binary data file ER Mapper™ grid ASCII header file <i>NN = layer number 01→30</i> <i>units=S/m, 30 grids, 150 files</i>
.\grids\log_layers\ log_conductivity_NN log_conductivity_NN.ers	logarithmic layer conductivity grids ER Mapper™ grid binary data file ER Mapper™ grid ASCII header file <i>NN = layer number 01→30</i> <i>units=log10(S/m), 30 grids, 150 files</i>
.\grids\dslice\ dslice_DF_DT dslice_DF_DT.ers	depth slice conductivity grids ER Mapper™ grid binary data file ER Mapper™ grid ASCII header file <i>DF = slice top depth metres below surface</i> <i>DT = slice bottom depth metres below surface</i> <i>units=S/m, 23 grids, 92 files</i>
.\grids\log_dslice\ log_dslice_DF_DT log_dslice_DF_DT.ers	logarithmic depth slice conductivity grids ER Mapper™ grid binary data file ER Mapper™ grid ASCII header file <i>DF = slice top depth metres below surface</i> <i>DT = slice bottom depth metres below surface</i> <i>units=log10(S/m), 23 grids, 150 files</i>

<p>.\grids\eslice\ dslice_sEF_sET dslice_sEF_sET.ers</p>	<p>elevation slice conductivity grids ER Mapper™ grid binary data file ER Mapper™ grid ASCII header file <i>s = p/m (plus/minus) above/below sea level</i> <i>EF = slice bottom elevation relative sea level</i> <i>ET = slice top elevation relative sea level</i> <i>units=S/m, 49 grids, 196 files</i></p>
<p>.\grids\log_eslice\ log_eslice_sEF_sET log_eslice_sEF_sET.ers</p>	<p>logarithmic elevation slice conductivity grids ER Mapper™ grid binary data file ER Mapper™ grid ASCII header file <i>s = p/m (plus/minus) above/below sea level</i> <i>EF = slice bottom elevation relative sea level</i> <i>ET = slice top elevation relative sea level</i> <i>units=log10(S/m), 49 grids, 196 files</i></p>
<p>.\grids\conductance\ conductance conductance.ers</p>	<p>conductance grid ER Mapper™ grid binary data file ER Mapper™ grid ASCII header file <i>total conductance 0 to 2000 m</i> <i>units=S/m, 1 grid, 5 files</i></p>
<p>.\grids\other\ iterations, iterations.ers lambda, lambda.ers phid, phid.ers phim, phim.ers phic, phic.ers phis, phis.ers</p>	<p>ancillary inversion outputs number of inversion iterations λ regularisation factor Φ_d data misfit term Φ_m model misfit tterm Φ_c conductivity misfit term Φ_s smoothness misfit term <i>ER Mapper™ grid binary data and header (.ers)</i> <i>6 grids, 30 files</i></p>
<p>.\multiplots\ lei_multiplot_LLLLL.pdf lei_multiplot_LLLLL.jpg</p>	<p>graphical multiplots showing inversion sections PDF format multplot JPEG format multplot <i>LLLL = flight line number</i> <i>211 flight lines, 422 files</i></p>
<p>.\georeferenced_sections\ LLLLL.jpg LLLLL.jgw colourbar.jpg colourbar.tif</p>	<p>graphical georeferenced sections JPEG image file for the georeference section world file that georeferences the section JPEG colour bar for the sections TIFF colour bar for the sections <i>LLLL = flight line number</i> <i>211 flight lines, 422 files</i></p>
<p>.\waveform\ VTEM.cfm VTEM.vfm</p>	<p>waveform files ASCII transmitter current waveform file ASCII receiver voltage waveform file</p>

Appendix E Point located data header file

```

COMM Kombolgie VTEM AEM Survey, Northern Territory, 2008.
COMM Geoscience Australia Project 1195
COMM
COMM Geoscience Australia Layered Earth Inversion Data
COMM GeoCat# 72582
COMM
COMM This file is the metadata file for the accompanying
COMM ASCII columns data file kombolgie_lei.dat
COMM
COMM Before using this product users are advised to carefully read the
COMM report "Kombolgie VTEM AEM Survey: Inversion Report" in the
COMM accompanying digital data package (file: kombolgie LEI_report.pdf).
COMM The report details important considerations that users should take
COMM into account when interpreting the data. These considerations relate
COMM to non-uniqueness, noise and data misfit.
COMM
COMM Intrepid ASEG-GDF2 Export
COMM PROJ GDA94 / MGA zone 53          GRS 1980          6378137.0000
298.257222 0.000000 Transverse Mercator 0.000000 135.000000
0.999600 500000.000000 1000000.000000
COMM
COMM Col# Channel          Units Description
Format Undefined
COMM ---- -
-----
COMM 1 project          NA GA project number
I4 9999
COMM 2 date            NA date flown
I9 9999
COMM 3 flight          NA flight number
I5 9999
COMM 4 line            NA line number
I6 9999
COMM 5 fid             NA fiducial
F9.2 9999
COMM 6 easting         m GDA94-MGA53 easting
F11.2 9999
COMM 7 northing        m GDA94-MGA53 northing
F11.2 9999
COMM 8 elevation       m ground elevation above sea level
F8.2 9999
COMM 9 altimeter       m altimeter on helicopter
F8.2 9999
COMM 10 tx_height      m transmitter loop height
F8.2 9999
COMM 11 nlayers        NA number of inversion layers
I3 9999
COMM 12 conductivity_01 S/m layer 01 conductivity
F11.7 9999
COMM 13 conductivity_02 S/m layer 02 conductivity
F11.7 9999
COMM 14 conductivity_03 S/m layer 03 conductivity
F11.7 9999
COMM 15 conductivity_04 S/m layer 04 conductivity
F11.7 9999
COMM 16 conductivity_05 S/m layer 05 conductivity
F11.7 9999
COMM 17 conductivity_06 S/m layer 06 conductivity
F11.7 9999
COMM 18 conductivity_07 S/m layer 07 conductivity
F11.7 9999
COMM 19 conductivity_08 S/m layer 08 conductivity
F11.7 9999
COMM 20 conductivity_09 S/m layer 09 conductivity
F11.7 9999
COMM 21 conductivity_10 S/m layer 10 conductivity
F11.7 9999
COMM 22 conductivity_11 S/m layer 11 conductivity
F11.7 9999
COMM 23 conductivity_12 S/m layer 12 conductivity
F11.7 9999
COMM 24 conductivity_13 S/m layer 13 conductivity
F11.7 9999

```

Kombolgie VTEM™ AEM Survey: Inversion Report

COMM 25	conductivity_14	S/m	layer 14 conductivity
F11.7	99999		
COMM 26	conductivity_15	S/m	layer 15 conductivity
F11.7	99999		
COMM 27	conductivity_16	S/m	layer 16 conductivity
F11.7	99999		
COMM 28	conductivity_17	S/m	layer 17 conductivity
F11.7	99999		
COMM 29	conductivity_18	S/m	layer 18 conductivity
F11.7	99999		
COMM 30	conductivity_19	S/m	layer 19 conductivity
F11.7	99999		
COMM 31	conductivity_20	S/m	layer 20 conductivity
F11.7	99999		
COMM 32	conductivity_21	S/m	layer 21 conductivity
F11.7	99999		
COMM 33	conductivity_22	S/m	layer 22 conductivity
F11.7	99999		
COMM 34	conductivity_23	S/m	layer 23 conductivity
F11.7	99999		
COMM 35	conductivity_24	S/m	layer 24 conductivity
F11.7	99999		
COMM 36	conductivity_25	S/m	layer 25 conductivity
F11.7	99999		
COMM 37	conductivity_26	S/m	layer 26 conductivity
F11.7	99999		
COMM 38	conductivity_27	S/m	layer 27 conductivity
F11.7	99999		
COMM 39	conductivity_28	S/m	layer 28 conductivity
F11.7	99999		
COMM 40	conductivity_29	S/m	layer 29 conductivity
F11.7	99999		
COMM 41	conductivity_30	S/m	layer 30 conductivity
F11.7	99999		
COMM 42	thickness_01	m	layer 01 thickness
F8.2	99999		
COMM 43	thickness_02	m	layer 02 thickness
F8.2	99999		
COMM 44	thickness_03	m	layer 03 thickness
F8.2	99999		
COMM 45	thickness_04	m	layer 04 thickness
F8.2	99999		
COMM 46	thickness_05	m	layer 05 thickness
F8.2	99999		
COMM 47	thickness_06	m	layer 06 thickness
F8.2	99999		
COMM 48	thickness_07	m	layer 07 thickness
F8.2	99999		
COMM 49	thickness_08	m	layer 08 thickness
F8.2	99999		
COMM 50	thickness_09	m	layer 09 thickness
F8.2	99999		
COMM 51	thickness_10	m	layer 10 thickness
F8.2	99999		
COMM 52	thickness_11	m	layer 11 thickness
F8.2	99999		
COMM 53	thickness_12	m	layer 12 thickness
F8.2	99999		
COMM 54	thickness_13	m	layer 13 thickness
F8.2	99999		
COMM 55	thickness_14	m	layer 14 thickness
F8.2	99999		
COMM 56	thickness_15	m	layer 15 thickness
F8.2	99999		
COMM 57	thickness_16	m	layer 16 thickness
F8.2	99999		
COMM 58	thickness_17	m	layer 17 thickness
F8.2	99999		
COMM 59	thickness_18	m	layer 18 thickness
F8.2	99999		
COMM 60	thickness_19	m	layer 19 thickness
F8.2	99999		
COMM 61	thickness_20	m	layer 20 thickness
F8.2	99999		
COMM 62	thickness_21	m	layer 21 thickness
F8.2	99999		
COMM 63	thickness_22	m	layer 22 thickness
F8.2	99999		
COMM 64	thickness_23	m	layer 23 thickness
F8.2	99999		

Kombolgie VTEM™ AEM Survey: Inversion Report

COMM 65	thickness_24	m	layer 24 thickness
F8.2	99999		
COMM 66	thickness_25	m	layer 25 thickness
F8.2	99999		
COMM 67	thickness_26	m	layer 26 thickness
F8.2	99999		
COMM 68	thickness_27	m	layer 27 thickness
F8.2	99999		
COMM 69	thickness_28	m	layer 28 thickness
F8.2	99999		
COMM 70	thickness_29	m	layer 29 thickness
F8.2	99999		
COMM 71	z_window_predicted_05	pV/Am ⁴	inversion forward model window 5
F11.7	99999		
COMM 72	z_window_predicted_06	pV/Am ⁴	inversion forward model window 6
F11.7	99999		
COMM 73	z_window_predicted_07	pV/Am ⁴	inversion forward model window 7
F11.7	99999		
COMM 74	z_window_predicted_08	pV/Am ⁴	inversion forward model window 8
F11.7	99999		
COMM 75	z_window_predicted_09	pV/Am ⁴	inversion forward model window 9
F11.7	99999		
COMM 76	z_window_predicted_10	pV/Am ⁴	inversion forward model window 10
F11.7	99999		
COMM 77	z_window_predicted_11	pV/Am ⁴	inversion forward model window 11
F11.7	99999		
COMM 78	z_window_predicted_12	pV/Am ⁴	inversion forward model window 12
F11.7	99999		
COMM 79	z_window_predicted_13	pV/Am ⁴	inversion forward model window 13
F11.7	99999		
COMM 80	z_window_predicted_14	pV/Am ⁴	inversion forward model window 14
F11.7	99999		
COMM 81	z_window_predicted_15	pV/Am ⁴	inversion forward model window 15
F11.7	99999		
COMM 82	z_window_predicted_16	pV/Am ⁴	inversion forward model window 16
F11.7	99999		
COMM 83	z_window_predicted_17	pV/Am ⁴	inversion forward model window 17
F11.7	99999		
COMM 84	z_window_predicted_18	pV/Am ⁴	inversion forward model window 18
F11.7	99999		
COMM 85	z_window_predicted_19	pV/Am ⁴	inversion forward model window 19
F11.7	99999		
COMM 86	z_window_predicted_20	pV/Am ⁴	inversion forward model window 20
F11.7	99999		
COMM 87	z_window_predicted_21	pV/Am ⁴	inversion forward model window 21
F11.7	99999		
COMM 88	z_window_predicted_22	pV/Am ⁴	inversion forward model window 22
F11.7	99999		
COMM 89	z_window_predicted_23	pV/Am ⁴	inversion forward model window 23
F11.7	99999		
COMM 90	z_window_predicted_24	pV/Am ⁴	inversion forward model window 24
F11.7	99999		
COMM 91	z_window_predicted_25	pV/Am ⁴	inversion forward model window 25
F11.7	99999		
COMM 92	z_window_predicted_26	pV/Am ⁴	inversion forward model window 26
F11.7	99999		
COMM 93	z_window_predicted_27	pV/Am ⁴	inversion forward model window 27
F11.7	99999		
COMM 94	z_window_predicted_28	pV/Am ⁴	inversion forward model window 28
F11.7	99999		
COMM 95	z_window_predicted_29	pV/Am ⁴	inversion forward model window 29
F11.7	99999		
COMM 96	z_window_predicted_30	pV/Am ⁴	inversion forward model window 30
F11.7	99999		
COMM 97	phid	NA	data misfit
F11.7	99999		
COMM 98	phim	NA	total model misfit term
F11.7	99999		
COMM 99	phic	NA	conductivity term
F11.7	99999		
COMM 100	phit	NA	thickness term - not used
F11.7	99999		
COMM 101	phig	NA	geometry term - not used
F11.7	99999		
COMM 102	phis	NA	smoothness term
F11.7	99999		
COMM 103	lambda	NA	regularisation factor
F11.7	99999		
COMM 104	alphac	NA	conductivity term weight
F11.7	99999		

Kombolgie VTEM™ AEM Survey: Inversion Report

COMM 105	alphat	NA	thickness term weight- not used
F11.7	99999		
COMM 106	alphag	NA	geometry term weight - not used
F11.7	99999		
COMM 107	alphas	NA	smoothness term
F11.7	99999		
COMM 108	iterations	NA	number of iterations
I4	999		
COMM 109	conductance	S	total conductance - 0-2000m
F11.6	99999		
COMM 110	dslice_0000_0020	S/m	depth slice 0000 to 0020 m below surface
F11.7	99999		
COMM 111	dslice_0020_0040	S/m	depth slice 0020 to 0040 m below surface
F11.7	99999		
COMM 112	dslice_0040_0060	S/m	depth slice 0040 to 0060 m below surface
F11.7	99999		
COMM 113	dslice_0060_0080	S/m	depth slice 0060 to 0080 m below surface
F11.7	99999		
COMM 114	dslice_0080_0100	S/m	depth slice 0080 to 0100 m below surface
F11.7	99999		
COMM 115	dslice_0100_0150	S/m	depth slice 0100 to 0150 m below surface
F11.7	99999		
COMM 116	dslice_0150_0200	S/m	depth slice 0150 to 0200 m below surface
F11.7	99999		
COMM 117	dslice_0200_0250	S/m	depth slice 0200 to 0250 m below surface
F11.7	99999		
COMM 118	dslice_0250_0300	S/m	depth slice 0250 to 0300 m below surface
F11.7	99999		
COMM 119	dslice_0300_0350	S/m	depth slice 0300 to 0350 m below surface
F11.7	99999		
COMM 120	dslice_0350_0400	S/m	depth slice 0350 to 0400 m below surface
F11.7	99999		
COMM 121	dslice_0400_0450	S/m	depth slice 0400 to 0450 m below surface
F11.7	99999		
COMM 122	dslice_0450_0500	S/m	depth slice 0450 to 0500 m below surface
F11.7	99999		
COMM 123	dslice_0500_0600	S/m	depth slice 0500 to 0600 m below surface
F11.7	99999		
COMM 124	dslice_0600_0700	S/m	depth slice 0600 to 0700 m below surface
F11.7	99999		
COMM 125	dslice_0700_0800	S/m	depth slice 0700 to 0800 m below surface
F11.7	99999		
COMM 126	dslice_0800_0900	S/m	depth slice 0800 to 0900 m below surface
F11.7	99999		
COMM 127	dslice_0900_1000	S/m	depth slice 0900 to 1000 m below surface
F11.7	99999		
COMM 128	dslice_1000_1200	S/m	depth slice 1000 to 1200 m below surface
F11.7	99999		
COMM 129	dslice_1200_1400	S/m	depth slice 1200 to 1400 m below surface
F11.7	99999		
COMM 130	dslice_1400_1600	S/m	depth slice 1400 to 1600 m below surface
F11.7	99999		
COMM 131	dslice_1600_1800	S/m	depth slice 1600 to 1800 m below surface
F11.7	99999		
COMM 132	dslice_1800_2000	S/m	depth slice 1800 to 2000 m below surface
F11.7	99999		
COMM 133	eslice_p0400_p0450	S/m	elevation slice +0400 to +0450 relative to sea
level F11.7	99999		
COMM 134	eslice_p0350_p0400	S/m	elevation slice +0350 to +0400 relative to sea
level F11.7	99999		
COMM 135	eslice_p0300_p0350	S/m	elevation slice +0300 to +0350 relative to sea
level F11.7	99999		
COMM 136	eslice_p0250_p0300	S/m	elevation slice +0250 to +0300 relative to sea
level F11.7	99999		
COMM 137	eslice_p0200_p0250	S/m	elevation slice +0200 to +0250 relative to sea
level F11.7	99999		
COMM 138	eslice_p0150_p0200	S/m	elevation slice +0150 to +0200 relative to sea
level F11.7	99999		
COMM 139	eslice_p0100_p0150	S/m	elevation slice +0100 to +0150 relative to sea
level F11.7	99999		
COMM 140	eslice_p0050_p0100	S/m	elevation slice +0050 to +0100 relative to sea
level F11.7	99999		
COMM 141	eslice_p0000_p0050	S/m	elevation slice +0000 to +0050 relative to sea
level F11.7	99999		
COMM 142	eslice_m0050_p0000	S/m	elevation slice -0050 to +0000 relative to sea
level F11.7	99999		
COMM 143	eslice_m0100_m0050	S/m	elevation slice -0100 to -0050 relative to sea
level F11.7	99999		
COMM 144	eslice_m0150_m0100	S/m	elevation slice -0150 to -0100 relative to sea
level F11.7	99999		

Kombolgie VTEM™ AEM Survey: Inversion Report

COMM 145	eslice m0200_m0150	S/m	elevation slice -0200 to -0150 relative to sea
level	F11.7 99999		
COMM 146	eslice m0250_m0200	S/m	elevation slice -0250 to -0200 relative to sea
level	F11.7 99999		
COMM 147	eslice m0300_m0250	S/m	elevation slice -0300 to -0250 relative to sea
level	F11.7 99999		
COMM 148	eslice m0350_m0300	S/m	elevation slice -0350 to -0300 relative to sea
level	F11.7 99999		
COMM 149	eslice m0400_m0350	S/m	elevation slice -0400 to -0350 relative to sea
level	F11.7 99999		
COMM 150	eslice m0450_m0400	S/m	elevation slice -0450 to -0400 relative to sea
level	F11.7 99999		
COMM 151	eslice m0500_m0450	S/m	elevation slice -0500 to -0450 relative to sea
level	F11.7 99999		
COMM 152	eslice m0550_m0500	S/m	elevation slice -0550 to -0500 relative to sea
level	F11.7 99999		
COMM 153	eslice m0600_m0550	S/m	elevation slice -0600 to -0550 relative to sea
level	F11.7 99999		
COMM 154	eslice m0650_m0600	S/m	elevation slice -0650 to -0600 relative to sea
level	F11.7 99999		
COMM 155	eslice m0700_m0650	S/m	elevation slice -0700 to -0650 relative to sea
level	F11.7 99999		
COMM 156	eslice m0750_m0700	S/m	elevation slice -0750 to -0700 relative to sea
level	F11.7 99999		
COMM 157	eslice m0800_m0750	S/m	elevation slice -0800 to -0750 relative to sea
level	F11.7 99999		
COMM 158	eslice m0850_m0800	S/m	elevation slice -0850 to -0800 relative to sea
level	F11.7 99999		
COMM 159	eslice m0900_m0850	S/m	elevation slice -0900 to -0850 relative to sea
level	F11.7 99999		
COMM 160	eslice m0950_m0900	S/m	elevation slice -0950 to -0900 relative to sea
level	F11.7 99999		
COMM 161	eslice m1000_m0950	S/m	elevation slice -1000 to -0950 relative to sea
level	F11.7 99999		
COMM 162	eslice m1050_m1000	S/m	elevation slice -1050 to -1000 relative to sea
level	F11.7 99999		
COMM 163	eslice m1100_m1050	S/m	elevation slice -1100 to -1050 relative to sea
level	F11.7 99999		
COMM 164	eslice m1150_m1100	S/m	elevation slice -1150 to -1100 relative to sea
level	F11.7 99999		
COMM 165	eslice m1200_m1150	S/m	elevation slice -1200 to -1150 relative to sea
level	F11.7 99999		
COMM 166	eslice m1250_m1200	S/m	elevation slice -1250 to -1200 relative to sea
level	F11.7 99999		
COMM 167	eslice m1300_m1250	S/m	elevation slice -1300 to -1250 relative to sea
level	F11.7 99999		
COMM 168	eslice m1350_m1300	S/m	elevation slice -1350 to -1300 relative to sea
level	F11.7 99999		
COMM 169	eslice m1400_m1350	S/m	elevation slice -1400 to -1350 relative to sea
level	F11.7 99999		
COMM 170	eslice m1450_m1400	S/m	elevation slice -1450 to -1400 relative to sea
level	F11.7 99999		
COMM 171	eslice m1500_m1450	S/m	elevation slice -1500 to -1450 relative to sea
level	F11.7 99999		
COMM 172	eslice m1550_m1500	S/m	elevation slice -1550 to -1500 relative to sea
level	F11.7 99999		
COMM 173	eslice m1600_m1550	S/m	elevation slice -1600 to -1550 relative to sea
level	F11.7 99999		
COMM 174	eslice m1650_m1600	S/m	elevation slice -1650 to -1600 relative to sea
level	F11.7 99999		
COMM 175	eslice m1700_m1650	S/m	elevation slice -1700 to -1650 relative to sea
level	F11.7 99999		
COMM 176	eslice m1750_m1700	S/m	elevation slice -1750 to -1700 relative to sea
level	F11.7 99999		
COMM 177	eslice m1800_m1750	S/m	elevation slice -1800 to -1750 relative to sea
level	F11.7 99999		
COMM 178	eslice m1850_m1800	S/m	elevation slice -1850 to -1800 relative to sea
level	F11.7 99999		
COMM 179	eslice m1900_m1850	S/m	elevation slice -1900 to -1850 relative to sea
level	F11.7 99999		
COMM 180	eslice m1950_m1900	S/m	elevation slice -1950 to -1900 relative to sea
level	F11.7 99999		
COMM 181	eslice m2000_m1950	S/m	elevation slice -2000 to -1950 relative to sea
level	F11.7 99999		

Appendix F Datum and projection

All products in the digital data package are spatially referenced according to the following geodetic datum and reference system.

Projection Name:	Map Grid of Australia, Zone 53 (MGA53)
Units:	metres
Datum:	Geocentric Datum of Australia 1994 (GDA94)
Epoch:	1994.0
Ellipsoid:	GRS80
Semi-major axis (a):	6 378 137.0 metres
Inverse flattening (1/f):	298.2572221
Central meridian:	135°00'00''
False Easting:	500 000 metres
False Northing:	10 000 000 metres